Quantitative evaluation of caprock sealing controlled by fault activity and hydrocarbon accumulation response: K gasfield in the Xihu Depression, East China Sea Basin

Fuwei Wang [a,b], Dongxia Chen [a,b,*], Qiaochu Wang [a,b], Wenlei Du [a,b], Siyuan Chang [a,b], Cheng Wang [a,b], Ziye Tian [a,b], Ming Cheng [a,b], Dongsheng Yao [a,b]

[a] *State Key Laboratory of Petroleum Resources and Prospecting, China University of Petroleum (Beijing), Beijing, 102249, China*
[b] *College of Geosciences, China University of Petroleum (Beijing), Beijing, 102249, China*

ABSTRACT

Caprock-sealing capability affected by fault activity is an important problem that needs to be resolved in hydrocarbon accumulation analysis, especially for rifted basins. In this article, a quantitative model based on the mechanical properties estimated by geophysical logging was first established to characterize the brittle-ductile transition of mudstone caprocks. By establishing a burial depth reconstruction model, the brittle-ductile stage of the mudstone caprock at the termination time of fault activity (TTFA) was restored. Moreover, the caprock juxtaposition thickness (CJT) for brittle rock and the shale smear factor (SSF) for brittle-ductile rock were selected to quantitatively describe the sealing capacity of caprock controlled by faults. These mathematical methods were finally applied to a case study of the K gasfield in the Xihu Depression, East China Sea Basin. Compared with the sealing characterization based on the current mechanical properties, the brittle-ductile reconstruction at the TTFA and matching sealing evaluation better describe the effectiveness of the mudstone caprock. Additionally, the quantified sealing capacity and corresponding hydrocarbon response indicate that a CJT value of 56.1 m and an SSF value of 3.0 can be the threshold for caprock sealing and nonsealing in the study area. As a result, caprock with poor sealing led to vertical hydrocarbon leakage in the structural low zone and structural high zone, while strong sealing caprock located in the structural center zone effectively prevented the upward migration of hydrocarbons, thereby controlling the vertical hydrocarbon distribution in the K gasfield. In general, the evaluation accuracy of caprock sealing predominantly relies on the geological input to the model, especially the fluid pressure, rock mechanical parameters, and caprock and fault interpretation results, and it is also affected by further uncertainties arising from the sealing threshold definition and structural uplift.

1. Introduction

Caprocks with low permeability (or high capillary pressure) are effective top seals for hydrocarbon accumulation in petroliferous basins (Dott and Reynolds, 1969; Schowalter, 1981; Watts, 1987; Jin et al., 2014). The effectiveness of the caprock affects the preservation of giant hydrocarbon reservoirs worldwide, such as the oil and gas fields distributed in the Tertiary basins of the Far East (Grunau, 1987), Arabian Basin of the Arabian Sea (Pierce, 1993), Vienna Basin of Austria (Fuchs and Hamilton, 2006), Bohai Bay Basin of China (Xue and Wang, 2020), and basins around the South China Sea (Wu et al., 2013). Therefore, the study of caprock sealing is of considerable importance in the analysis of hydrocarbon accumulation and preservation.

In principle, the sealing capacity of the caprock varies dynamically throughout its geological history, gradually enhancing with the continual burial process, but may be diminished or completely destroyed in later geological events (He and Zhang, 1997; Jin et al., 2013). The failure of caprock sealing can be genetically divided into three major mechanisms: capillary leakage (Schowalter, 1979; Watts, 1987), hydraulic fracturing (Watts, 1987; Engelder and Lacazette, 1990) and the episodic movement of faults induced by tectonic motion and/or overpressure (Gartrell et al., 2006; Manzocchi et al., 2010; Hao et al., 2015). For the laterally continuous cap layer, the sealing capacity of caprock can be statically evaluated by parameters, such as porosity,

---

permeability, pore throat radius, and capillary pressure (Lü et al., 1996; Ingram et al., 1997); therefore, the dynamic evolution of caprock sealing can be further analyzed by reconstructing capillary pressure (Gutierrez et al., 2000; Nygard et al., 2006; Jin et al., 2014). Moreover, from the perspective of hydraulic fracturing, the effective differential stress and rock tensile strength can be combined to reveal the seal failure caused by overpressure (Watts, 1987; Engelder and Lacazette, 1990; Sibson, 1996; Caillet et al., 1997) and to evaluate the risk of hydraulic fracturing in critical geological periods through overpressure evolution reconstruction (Hao et al., 2015). However, the evaluation of caprock sealing in rifted basins or regions with developed faults is generally more complicated, as shear deformation during faulting tends to destroy the continuity of the caprock.

Generally, the continual faulting process will gradually diminish or completely destroy the continuity of the caprock (Ingram and Urai, 1999; Faerseth, 2006; Fu et al., 2019). The related shear deformation during the faulting process predominantly depends on the mechanical properties of the caprock, which usually changes significantly with increasing burial depth (Hamami, 1999; Fuenkajorn et al., 2012; Alqahtani et al., 2013). On the whole, normal consolidated rock that has been continuously buried but never uplifted generally undergoes three deformation stages: brittle, brittle-ductile and ductile (Runar et al., 2006; Wang et al., 2019). To analyze the destruction from the fault to the continuity of the caprock, two effective parameters have been proposed for static-sealing quantitative evaluation. One is the caprock juxtaposition thickness (CJT) (Lü et al., 2007) for brittle rock, and the other is the shale smear factor (SSF) (Lindsay et al., 1993) for brittle-ductile rock. Unfortunately, current studies and methods on caprock sealing controlled by faults are all focused on the present day brittle-ductile properties and sealing evaluation (Fu et al., 2015; Wang et al., 2019) but fail to involve the dynamic effects of fault activity on caprock sealing. Theoretically, caprock sealing controlled by faults varies with the brittle-ductile properties of the caprock in geological history. However, the shear deformation of the caprock predominantly depends on its mechanical properties during the fault active duration instead of the current duration because fault sliding ceases at the termination of fault activity. Therefore, the caprock sealing evaluation based on the current mechanical properties does not accurately address the effectiveness of analysis of caprock. As the dynamic aspects of sealing capability are an important foundation for analyzing hydrocarbon accumulation and preservation, further dynamic evaluation and systematic quantitative research are still required to increase the accuracy of caprock-sealing evaluation, thereby reducing the hydrocarbon exploration risk in rifted basins.

Taking the K gasfield in the Xihu Depression in the East China Sea Basin as an example, this article aims to quantitatively reconstruct and evaluate the sealing capacity of mudstone caprock at the termination time of fault activity (TTFA), so as to reveal its hydrocarbon accumulation response. Two models were established to restore the brittle-ductile stage of caprock at the TTFA. One is a model for the critical conditions of the brittle-ductile transition, and the other is a reconstruction model of the paleoburial depth of the mudstone caprock at the TTFA. Furthermore, the caprock juxtaposition thickness (CJT) for brittle rock and the shale smear factor (SSF) for brittle-ductile rock were then selected to quantitatively describe the sealing capacity of caprock. These models and methods were applied to the K gasfield in the Xihu Depression, where Paleogene strata have developed three sets of regional mudstone caprocks: the Upper Huagang Formation (E_3h_1), Upper Pinghu Formation (E_2p_1) and Lower Pinghu Formation (E_2p_3). In this way, the sealing effectiveness of mudstone caprock under the control of fault activity and its hydrocarbon accumulation response are systematically analyzed.

2. Geological setting

The Xihu Depression is located in the northeastern East China Sea Basin and occupies a surface area of approximately 46,000 km^2 (Duan et al., 2017; Zhang et al., 2018) (Fig. 1a). It is surrounded by the Hupijiao, Haijiao, and Yushan Uplifts in the west and the Diaoyu Islands Uplift in the east (Fig. 1b). Generally, the tectonic evolution of the Xihu Depression consisted of a rifting stage (65.0–32.0 Ma), a thermal depression stage (32.0–5.0 Ma) and a regional subsidence stage (5.0 Ma-present) (Ye et al., 2007; Zhang et al., 2009) (Fig. 2). During the rifting stage, the basin experienced major tectonic events involving the Oujiang and Yuquan movements and formed fault systems characterized by two major trends, NNE-NE and NNW-EW (Song et al., 2010; Abbas et al., 2018). Moreover, a series of grabens developed along the major faults after the Huagang Movement and Longjing Movement during the thermal depression stage, and then the Xihu Depression entered a stage of regional subsidence in the Pliocene that continued until the Quaternary.

The sediments in the Xihu Depression are mainly composed of fluvial-delta-lacustrine, fjord-tidal flat, and shallow marine deposits (Abbas et al., 2018). They have been divided into different stratigraphic units comprising from bottom to top the Paleogene Baoshi (E_2b), Pinghu (E_2p) and Huagang (E_3h) formations; the Neogene Longjing, Yuquan, Liulang, and Santan formations; and the Quaternary Donghai Formation (Fig. 2). However, only the E_2b, E_2p and E_3h formations had most of the hydrocarbon accumulation and thus became the focus of petroleum exploration. The E_2b Formation is composed of siltstone and mudstone divided into two members, E_2b_1 and E_2b_2, which can provide favorable reservoirs for oil and gas accumulation. The E_2p Formation formed in a fjord-tidal flat sedimentary environment containing the main source and reservoir rocks and can be further subdivided into three members, E_2p_3, E_2p_2, and E_2p_1 from bottom to top (Xu et al., 2020). The E_3h Formation is dominated by fluvial-delta-lacustrine deposits and forms laterally connected sandstone bodies and mudstone caprock (Zhang et al., 2018), which effectively prevents the vertical migration of hydrocarbons.

This research focuses on the K gasfield of the Pinghu Slope Belt, which is located in the central West Slope Belt (WSB) in the Xihu Depression (Fig. 1b and c). The hydrocarbons discovered thus far in the K gasfield are mainly natural gas, condensate and light oils (Shan et al., 2015; Su et al., 2015), which are charged from the local mature source rocks and high-to overmature source rocks of the Western Sub Sag (WSS) (Ye et al., 2007; Shan et al., 2015; Zhang et al., 2018; Su et al., 2020). According to the stratigraphic configurations of source-reservoir-seal rock units, there are three main petroleum systems in the K gasfield (Fig. 2). The deepest buried lower petroleum system is located in the E_2b interval, and the hydrocarbons generated from the local E_2b source rock and the E_2p_3 source rock in the WSS are sealed under the E_2p_3 mudstone caprock. The middle petroleum system located in the E_2p Formation has hydrocarbons charged from local E_2p_3 source rocks and the mature E_2p_3 source rock in the WSS, and are sealed below the E_2p_1 mudstone caprock. However, due to the absence of local mature source rock, the hydrocarbons of the upper petroleum system in the E_3h Formation came from the vertical leakage of underlying hydrocarbon accumulation through nonsealing caprock. In addition, the study area has developed normal fault systems dominated by NNE-NE trends (Cai and Zhang, 2013; Yang et al., 2014) (Fig. 1c), which are more likely to affect the sealing capacity of mudstone caprock. Based on the oil and gas discovered thus far, there are great variations in the vertical distribution of hydrocarbons along different normal faults (Shan et al., 2015; Wang et al., 2021), indicating the destructive effect of faults on mudstone caprock.

3. Data and evaluation methods

The systematic quantitative evaluation of caprock sealing controlled by fault activity consists of the following three major steps: (1) detailed spatial descriptions of the mudstone caprocks and faults by combining well logging and seismic data, (2) quantitative characterization of brittle-ductile transition behaviors of caprocks and their brittle-ductile
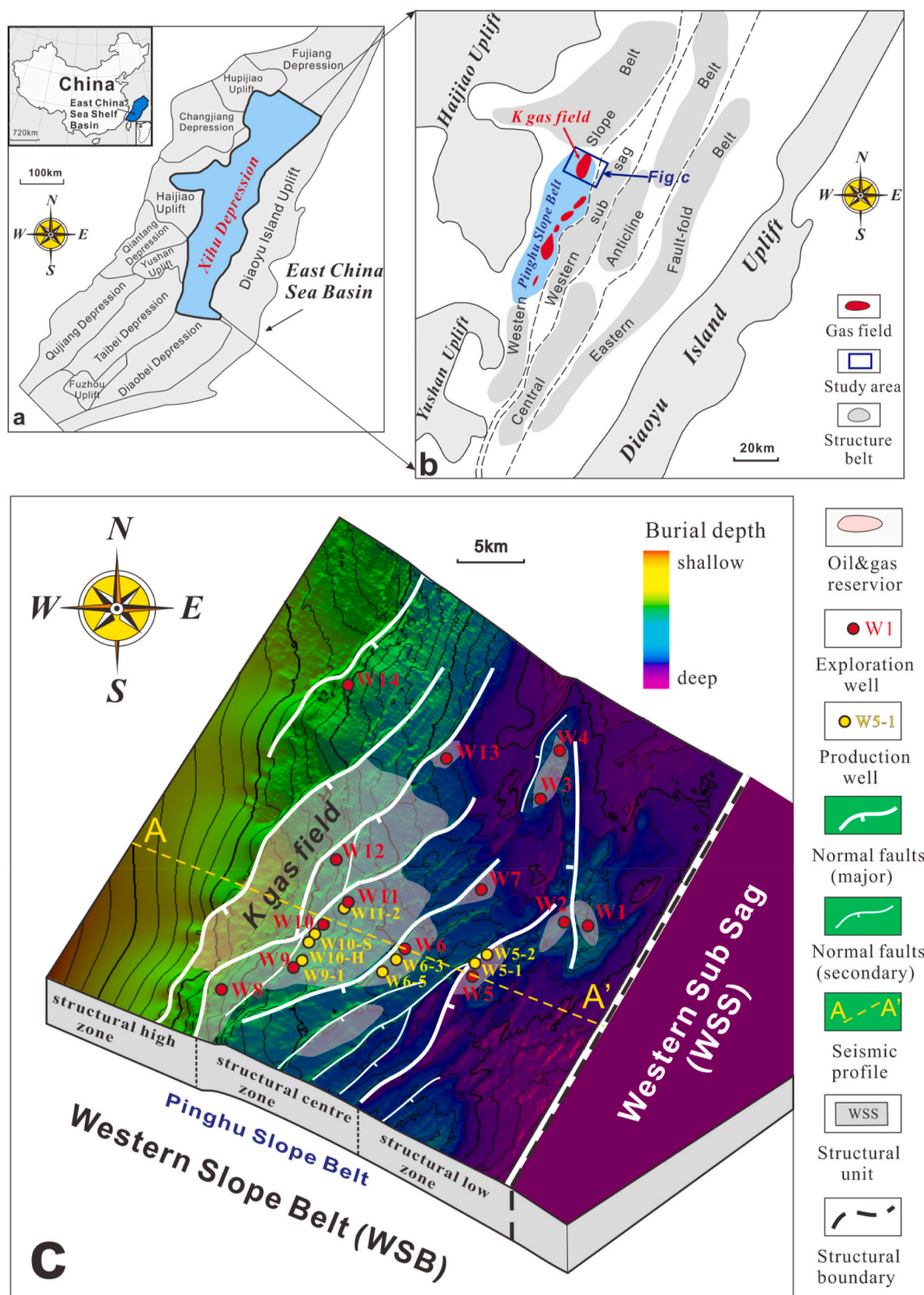
Fig. 1. (a) Tectonic map of the East China Sea Basin showing the location of the Xihu Depression. (b) Tectonic map of the Xihu Depression showing the location of the K gasfield. The study area is outlined by the blue box. (c) Structural map of the study area showing the normal fault systems, oil and gas reservoirs, exploration and production wells, and seismic profile. (For interpretation of the references to colour in this figure legend, the reader is referred to the Web version of this article.)

reconstruction in critical geological time, and (3) quantitative evaluation of the sealing capability of mudstone caprocks in different brittle-ductile stages.

3.1. Seismic and well-logging data and interpretation of caprocks and faults

The detailed spatial interpretation of faults and mudstone caprocks is a vital foundation for analyzing the effectiveness of caprock sealing under fault destruction. In this research, a high-resolution 3D seismic volume with a dominant frequency of 60 Hz was collected to determine
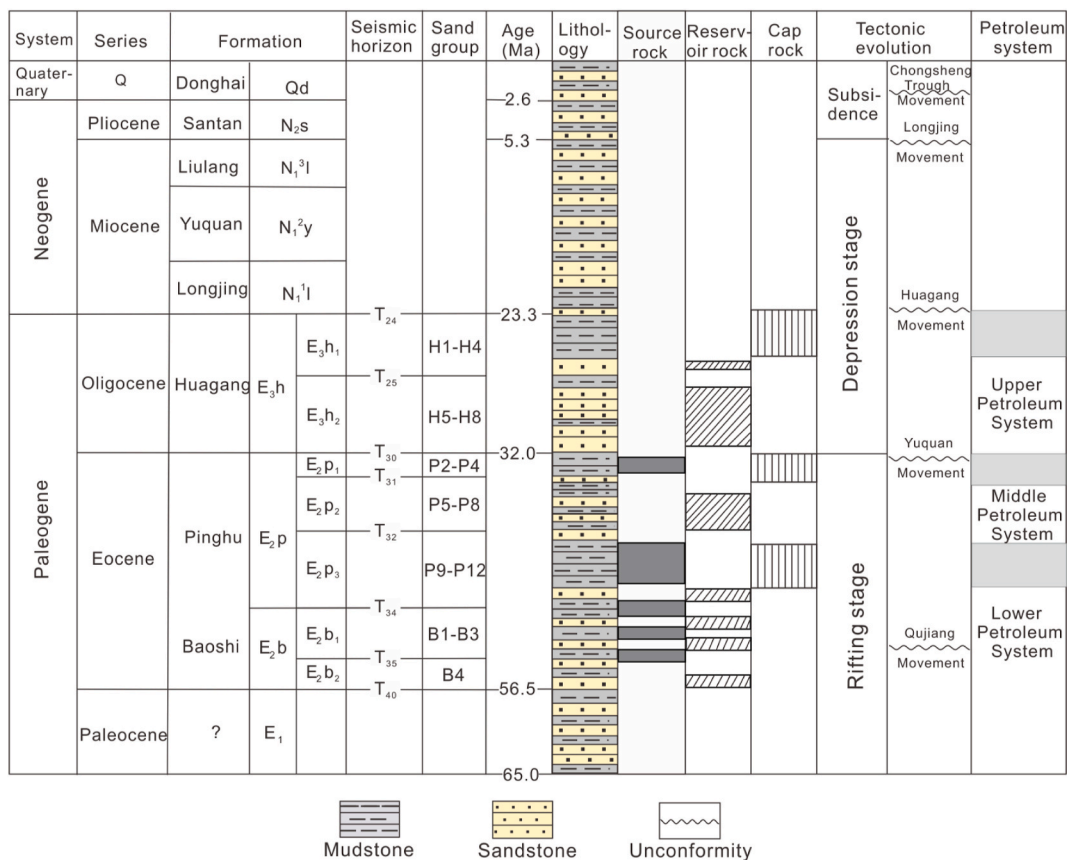
Fig. 2. Summary diagram showing the stratigraphy, source-reservoir-seal rock units, tectonic stages, and petroleum system in the K gasfield in the Xihu Depression.

the spatial distribution and displacements of normal faults developed in the K gasfield. The fault polygon interpretation and fault displacement (or throw) measurement were carried out using Petrel software provided by the Schlumberger Company (Fig. 3). Furthermore, lithological logging interpretation data from 14 single exploration wells (Fig. 1c) were used to determine the location of mudstone caprocks, and then the well structural profiles were established to describe the lateral variation of the mudstone layer (Fig. 3a). Because the limited well positions do not capture the spatial range of mudstone in the entire study area, under the constraints of the stratum reflection interface, the thickness of three
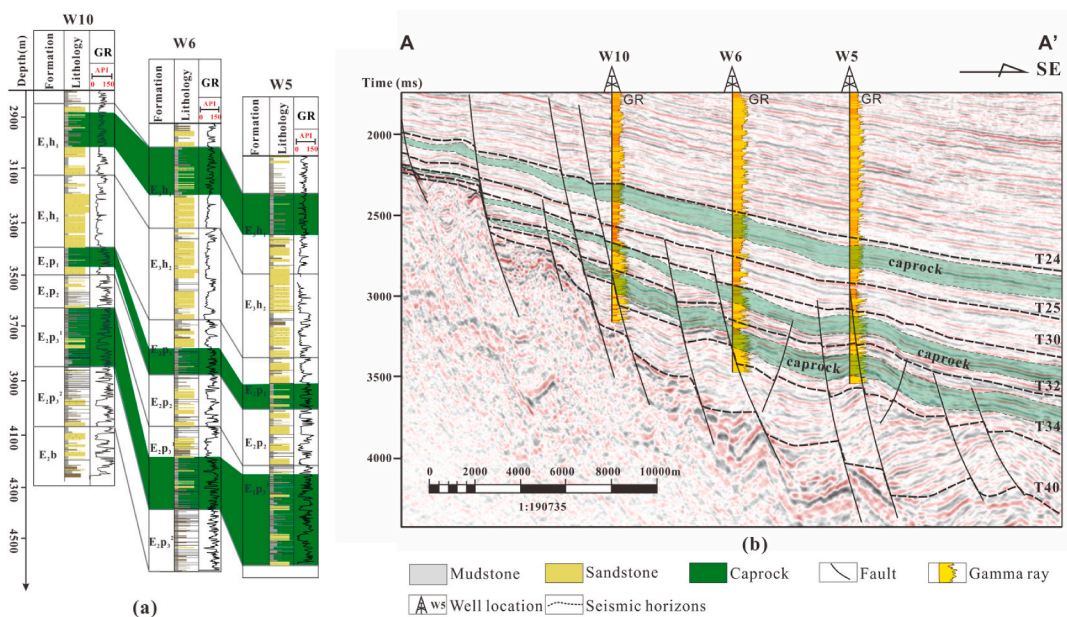
Fig. 3. (a) Well structural profile showing the mudstone caprock distribution in wells W10, Well W6 and Well W5. (b) The seismic profile AA′ showing the interpretation of mudstone caprock through seismic attribute tracking combined with logging lithological correction. The seismic interpretation horizons of T24, T25, T30, T32, T34, and T40 correspond to the top interface of E_3h_1, E_3h_2, E_2p_1, E_2p_3, E_2b_1 and E_1, respectively. See Fig. 1c for the location of profile AA′.

major mudstone caprocks is further obtained through seismic attribute tracking combined with logging lithological correction (Fig. 3b). In this way, the spatial distribution of normal faults and mudstone caprocks in the study area was systematically revealed. All above data were collected from the China National Offshore Oil Corporation (CNOOC) Research Institute and the SINOPEC Shanghai Offshore Oil & Gas Company.

3.2. Quantitative evaluation of the brittleness-ductility of mudstone caprock

The mechanical properties of the rock determine the deformation behavior of the caprock and the internal structural type of the fault zone during fault activity. Previous studies have confirmed that there are significant disparities in the deformation mechanisms and internal structure of the fault zone between brittle and ductile caprocks (Faerseth, 2006; Fu et al., 2015, 2019; Vrolijk et al., 2016). Based on the caprock deformation mechanism, quantities of fractures are formed in mudstone in the process of brittle deformation, while the caprock in the brittle-ductile (semibrittle) deformation stage is typically characterized by clay smearing. Therefore, determining the brittle-ductile transition behaviors of mudstone caprock is another important basis for revealing the caprock sealing capability and its dynamic variations.

3.2.1. Quantitative characterization of caprock brittle-ductile transition behaviors

The mechanical properties of rock vary with diagenesis, temperature, confining pressure, petrophysical characteristics, etc. (Hamami, 1999; Fuenkajorn et al., 2012; Alqahtani et al., 2013), but in general, normal consolidated rock that has been continuously buried but never uplifted goes through three transition stages, including brittle, brittle-ductile (semibrittle) and ductile (Fig. 4a). In this research, based on the method proposed by Kohlstedt et al. (1995), the Byerlee friction law and Goetze criterion were combined with the Mohr-Coulomb fracture envelope to quantitatively determine the caprock brittle-ductile transition behaviors (Fig. 4b).

According to the quantitative evaluation principle of Kohlstedt et al. (1995), the intersection of the Mohr-Coulomb fracture envelope and Byerlee's law curve represents the critical transition from the brittle to brittle-ductile stage, while the intersection of the Mohr-Coulomb fracture envelope and Goetze's criterion curve marks the beginning of the ductile stage (Fig. 4b). For these three basic curves, Byerlee's law and Goetze's criterion are more convenient to obtain under the principal stress coordinates. Byerlee's law describes a sliding friction relationship that does not rely on rock type and sliding surface characteristics (e.g., roughness) (Byerlee, 1968, 1978), which is universally applicable to various sliding friction in nature. In principal stress coordinates, Byerlee's law can be expressed as Equations (1) and (2). In addition, the

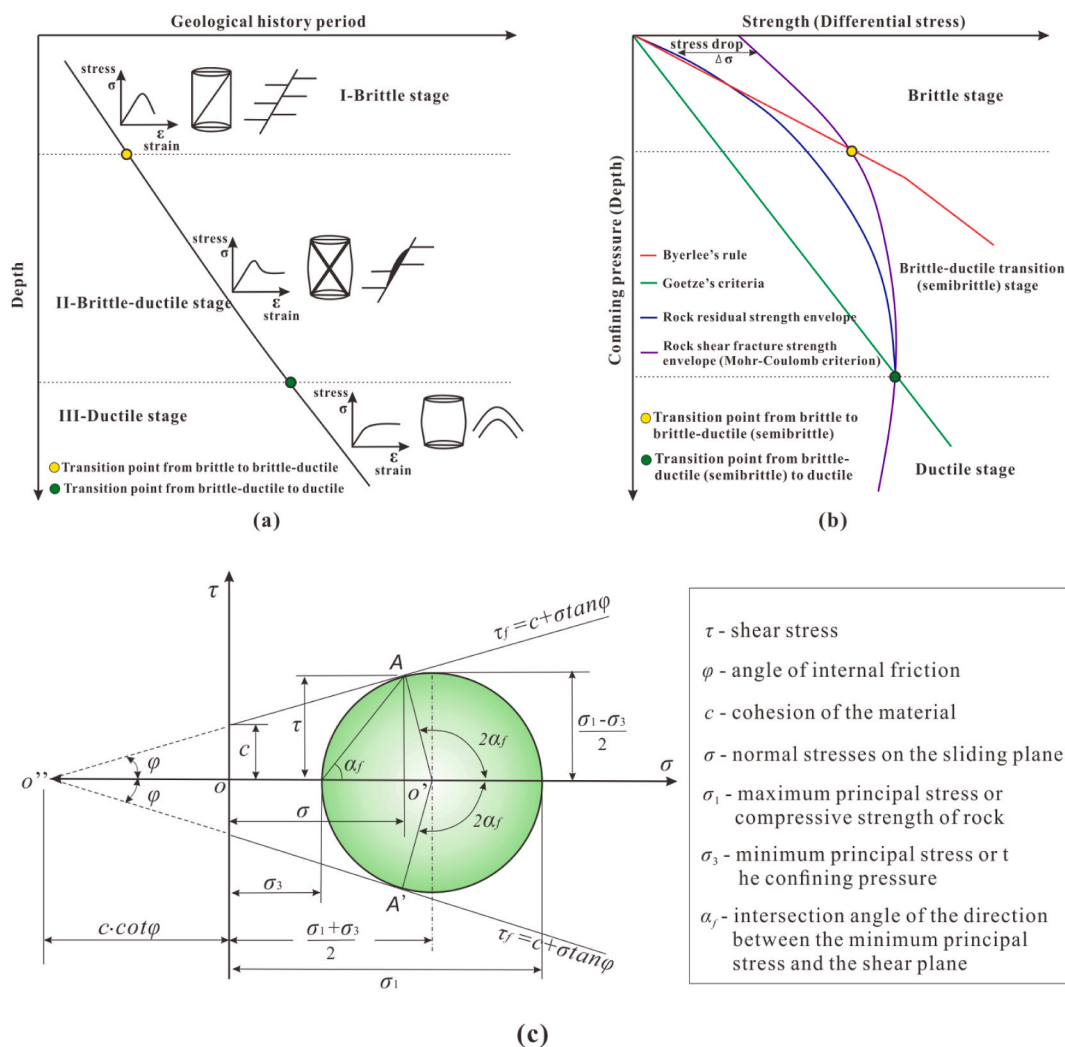**Fig. 4.** (a) Schematic diagram of the relationship between the burial history of normally consolidated rock and brittle-ductile transformation (after Wang et al., 2019). (b) Quantitative characterization method for the brittle-ductile transformation behaviors of caprock (after Kohlstedt et al., 1995; Wang et al., 2019). (c) The strength envelope of shear and normal stresses on the Mohr-Coulomb strength criterion (after Zhao, 2000).

difference between the rock fracture strength and residual strength is called the stress drop ($\Delta\sigma$), and the stress drop decreases gradually with increasing ductility (Fig. 4a and b). Thus, when the stress drop is zero, the rock exhibits obvious rheological characteristics, and no brittle fracture occurs. Under this condition, the rock fracture strength ($\sigma1$-$\sigma3$) is approximately equal to the effective confining pressure ($\sigma3$) (Goetze, 1971), and this empirical law is called Goetze's criterion and can be expressed as Equation (3).

$$\sigma1 - \sigma3 \approx 3.7\sigma3, \sigma3 < 100 \text{ MPa} \tag{1}$$

$$\sigma1 - \sigma3 \approx 2.1\sigma3 + 210, \sigma3 > 100 \text{ MPa} \tag{2}$$

$$\sigma1 - \sigma3 \approx \sigma3 \tag{3}$$

where $\sigma1$ is the maximum principal stress, MPa; and $\sigma3$ is the minimum principal stress, MPa.

However, compared with the two curves above, the Mohr-Coulomb fracture envelope is more difficult to set up. This envelope curve reflects the shear fracture strength ($\sigma1$-$\sigma3$) of the rock under various effective confining pressures ($\sigma3$) (Kohlstedt et al., 1995; Petley, 1999; Wang et al., 2019) (Fig. 4b). This curve requires a large number of rock mechanic experimental data of different mudstones to be obtained by quadratic fitting. However, offshore core samples are scarce and difficult to obtain, especially mudstone as a caprock. Therefore, there are obvious limitations in fitting the Mohr-Coulomb fracture envelope from experimental rock data when core samples are unavailable for laboratory testing. Based on the fact that many factors affecting rock mechanics also affect other physical properties, rock strength can be effectively estimated from geophysical logging data, such as porosity, velocity, and elastic modulus (McNally, 1987; Horsrud, 2001; Chang et al., 2006). Nevertheless, the empirical equations summarized thus far are only applicable to the acquisition of unconfined rock strength (Chang et al., 2006), and they cannot directly represent the fracture strength under different effective confining pressures. Therefore, we propose a new method and procedure based on geophysical logging to establish the Mohr-Coulomb fracture envelope of mudstone caprock, and the specific description is as follows.

Theoretically, the Mohr-Coulomb fracture envelope represents the limit equilibrium condition of the Mohr-Coulomb strength criterion (Fig. 4c), which meets the principal stress law shown in Equation (4) and Equation (5). Thus, when the effective confining pressure ($\sigma3$) and mechanical parameters (internal friction angle ϕ and rock cohesion C) of the given mudstone are all determined, the shear fracture strength ($\sigma1$-$\sigma3$) can be calculated and utilized to fit the Mohr-Coulomb fracture envelope. For the determination of effective confining pressure ($\sigma3$), previous studies have confirmed that the effective stress on the framework of porous media predominantly depends on the external stress and internal pore-fluid pressure in the media (Terzaghi, 1923; Bishop, 1959; Li et al., 1999). Therefore, for subsurface mudstone with different burial depths, the effective confining pressure acting on it can be equivalent to the difference between the overburden pressure (P_O) and pore-fluid pressure (P_F), as written in Equation (6). However, because the limited measured pore pressures (from the drill stem test and wireline formation test) cannot meet the evaluation requirements at different burial intervals, geophysical logging data (measured as sonic travel time) are applied as an efficient dataset for continuous pressure observation by using the equivalent depth method (Hottman and Johnson, 1965; Magara, 1968; Webster et al., 2011). On the other hand, the mechanical properties of subsurface mudstones at different depths can also be quantitatively determined through geophysical logging data. As shown in Equation (7), cohesion (C) is a function of the dynamic modulus of elasticity (E_d), shale volume content (V_{sh}), volume compression coefficient (C_b) and the constant m related to the angle of internal friction (ϕ) (Deere and Miller, 1966). E_d and C_b can be calculated from the logging curves of mudstone density (ρ_m), S-wave travel time (Δt_s) and P-wave travel time (Δt_p), as shown in equations (8)–(10)

(Wang et al., 2007). It is also convenient to estimate V_{sh} from the gamma-ray curve according to Equation (11) and Equation (12). Furthermore, the curve of P-wave velocity (V_p) can be used to estimate the internal friction angle (ϕ) of mudstone, as written in Equation (13) (Lal, 1999) and Equation (14). Finally, combined with the constant m determined by Equation (15) (Sun et al., 2016), the effective confining pressure and corresponding shear fracture strength of mudstone at different burial depths can be obtained, thus constructing the Mohr-Coulomb fracture envelope.

For the selection of data, because the current depth interval of the mudstone caprocks is insufficient to describe the Mohr-Coulomb fracture envelope that varies with burial depth, we also selected noncaprock mudstone with V_{sh} close to the mudstone caprock for calculations. Consequently, the critical confining pressure condition for the brittle-ductile transition can be effectively determined by combining the Mohr-Coulomb fracture envelope with the Byerlee friction law and Goetze criterion and finally converted to the corresponding burial depth. In this way, the brittle-ductile stage of mudstone caprocks with different burial depths is effectively determined.

$$\sigma_1 = \sigma_3 \frac{1 + \sin\phi}{1 - \sin\phi} + 2C \frac{\cos\phi}{1 - \sin\phi} \tag{4}$$

$$\sigma_1 - \sigma_3 = \sigma_3 \frac{2\sin\phi}{1 - \sin\phi} + 2C \frac{\cos\phi}{1 - \sin\phi} \tag{5}$$

$$\sigma_3 = P_O - P_F = \rho_m gh - P_F \tag{6}$$

$$C = \frac{0.025 m E_d}{C_b}\left(8V_{sh} + 4.5(1 - V_{sh})\right) \times 10^{-3} \tag{7}$$

$$E_d = \frac{\rho_m \left(3\Delta t_s^2 - 4\Delta t_p^2\right)}{\Delta t_s^2 \left(\Delta t_s^2 - \Delta t_p^2\right)} \tag{8}$$

$$\Delta t_s = \frac{\Delta t_p}{\left(1 - 1.15 \frac{\left(\frac{1}{\rho_m}\right) + \left(\frac{1}{\rho_m}\right)^3}{\left(\frac{1}{\rho_m}\right)_e}\right)^{1.5}} \tag{9}$$

$$C_b = \frac{3\Delta t_p^2 \Delta t_s^2}{\rho_m \left(3\Delta t_s^2 - 4\Delta t_p^2\right)} \tag{10}$$

$$V_{sh} = \frac{2^{GCUR \cdot V_{sh}'} - 1}{2^{GCUR} - 1} \tag{11}$$

$$V_{sh}' = \frac{GR - GR_{min}}{GR_{max} - GR_{min}} \tag{12}$$

$$\phi = sin^{-1}\left(\frac{V_p - 1000}{V_p + 1000}\right) \tag{13}$$

$$V_p = \frac{1}{\Delta t_p} \tag{14}$$

$$m = \frac{2\cos\phi}{1 - \sin\phi} \tag{15}$$

where $\sigma1$ is the maximum principal stress, MPa; $\sigma3$ is the minimum principal stress, MPa; ϕ is the rock internal friction angle, °; C is the cohesion of rock, MPa; P_O is the overburden pressure from sediments, MPa; P_F is the pore-fluid pressure of the mudstone, MPa; ρ_m is the rock density, g/cm³; g is gravitational acceleration, 9.8 m/s²; h is the thickness of the sediments above the mudstone caprock, m; m is the constant related to the angle of internal friction; E_d is the dynamic modulus of

elasticity, MPa; C_b is the volume compression coefficient of rock, MPa^{-1}; V_{sh} is the shale volume content, %; Δt_s is the S-wave travel time, µs/m; Δt_p is the P-wave travel time, µs/m; GCUR is the regional empirical co-efficient, 3.7 for Tertiary strata and 2 for the strata deposited before the Tertiary; GR_{max} and GR_{min} are the gamma values of pure mudstone and pure sandstone, respectively; and V_p is the P-wave velocity, m/µs.

3.2.2. Reconstruction of caprock brittleness-ductility at the termination time of fault activity (TTFA)

Since the shear deformation of the caprock no longer occurs with the termination of fault activity, the deformation characteristics of the mudstone caprock depend on its brittle-ductile properties during the fault active period rather than the current properties. Therefore, errors would occur when directly using the brittle-ductile properties determined by the current burial depth to assess the integrity or sealing ca-

pacity of the caprock. To characterize the effectiveness of the top seal more accurately, the mechanical properties of the caprock need to be restored to the fault active period for evaluation. However, as the movement of faults is generally episodic and cumulative (Blair and Bilodeau, 1988; Cartwright et al., 1995; Rykkelid and Fossen, 2002; Jackson and Rotevatn, 2013), it is difficult to obtain the exact time of each episodic fault movement throughout geological history. Considering that the shear deformation of the caprock will continue until the last activity of the fault, we choose the termination time of the last fault activity (TTFA) as the critical time point for the brittle-ductile reconstruction of caprock. Moreover, the burial depth at the top of the fault (h_{ft}) can provide a valid indication for the termination of the last fault activity (Fig. 5a).

The burial depth restoration of the mudstone caprock at the TTFA is the key to determining the paleobrittle-ductile characteristics. Theoretically, with increasing burial depth, overburden pressure leads to a
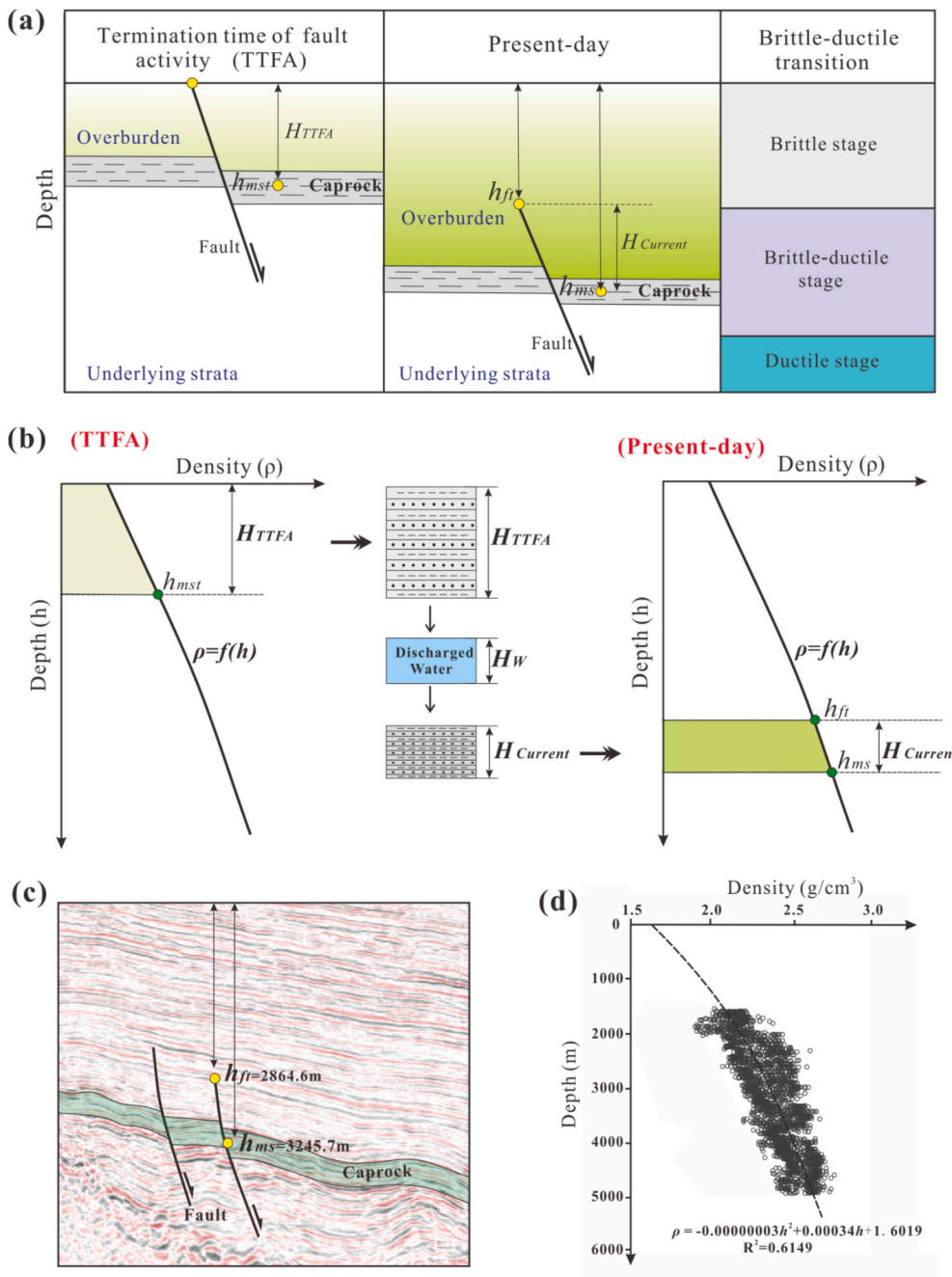

Fig. 5. (a) Conceptual diagram showing the brittle-ductile stage of the caprock at present and at the termination time of fault activity (TTFA). H_{TTFA} and $H_{Current}$ represent the thickness of the stratigraphic interval from the central position of the mudstone caprock to the top of the fault at the TTFA and the present, respectively. h_{ms} and h_{ft} represent the current burial depth of the mudstone caprock and the top of the fault, and h_{mst} is the paleoburial depth of the mudstone caprock at the TTFA. (b) The conceptual model showing the change in stratum thickness and density with burial depth at the TTFA and present. H_W represents the thickness of water discharged due to compaction after TTFA, and the corresponding mass and density mathematical models are shown in Equations (16)–(20). (c) An example of measuring the current burial depth of mudstone caprock (h_{ms}) and the top of the fault (h_{ft}). (d) The density-depth relationship of well W5 in the structural low zone.

reduction in porosity and loss of pore water, thereby reducing the thickness of the deposited formations. By establishing a normal compaction tendency, porosity or density logging can be applied to reconstruct the thickness changes of sedimentary layers during compaction history (Perrier and Quiblier, 1974; Yuan and Qian, 1986; Mou, 1993; Shao et al., 1999). Generally, the "slice" method has relatively high accuracy in determining the paleoburial depth of strata (Perrier and Quiblier, 1974), but it is not suitable for large-scale work where reconstruction time points vary over a wide range. Therefore, a simplified model was proposed in this article to quantitatively restore the paleoburial depth of the mudstone caprock at the TTFA.

Without considering chemical reactions (e.g., mineral transformation, dissolution and cementation), the depth, thickness, and porosity of the sedimentary layer vary continuously during normal compaction, but the solid mass remains unchanged (Mou, 1993). Assuming that the total mass of the sedimentary strata (solid and fluid) remains conserved before and after compaction, the thickness of sedimentary layers during the critical geological time can be restored by density logging curves, and the detailed steps are as follows. First, we defined the interval from the mudstone caprock (central position) to the top of the fault as an entire stratigraphic layer, and thus, the thickness of this stratigraphic interval at the TTFA (abbreviated as H_{TTFA}) is equivalent to the paleoburial depth of the mudstone caprock (abbreviated as h_{mst}) at the bottom position (Fig. 5a). In addition, the current thickness of the stratigraphic interval from the center of the mudstone caprock to the top of the fault (abbreviated as $H_{Current}$) can be determined by the current burial depth of the mudstone caprock (h_{ms}) and the top of the fault (h_{ft}). Based on the principle of constant mass of sedimentary materials, the total weight of the stratigraphic interval from the center of the mudstone caprock to the top of the fault at the TTFA should be equal to the current weight of the sedimentary interval plus the weight of the water that has been discharged, as shown in the geological model (Fig. 5b). In a given unit area, the mathematical model derived from the above geological model can be written as Equation (16) and combined with Equation (17) to obtain the relationship as Equation (18). Moreover, due to the sedimentary layer is continuously compacted as the burial depth increases, the bulk density is generally expressed as a function of depth ($D(h)$). Therefore, the average density of the stratigraphic interval (from the mudstone caprock to the top of the fault) on the present day and the TTFA can be obtained by the mathematical integration shown in Equation (19) and Equation (20), and the relevant burial depth can be measured by using the seismic interpretation section (Fig. 5c). On the other hand, the density compaction curve usually varies due to vertical lithological changes at different structural locations. Thus, the function of bulk density changing with burial depth ($D(h)$) needs to be fitted according to different locations, and Equation (21) is the bulk density variation function of well W5 located in the structural low zone (Fig. 5d). Once the function of $D(h)$ is established, by incorporating Equations (19)–(21) into Equation (18), the paleoburial depth of the mudstone caprock at the TTFA can be computed. In this way, the brittle-ductile stage of mudstone caprocks at the TTFA can be further determined by comparison with the critical burial depth of the brittle-ductile transition.

$$H_{TTFA} \cdot D_{TTFA} = H_{Current} \cdot D_{Current} + H_W \cdot D_W \qquad (16)$$

$$H_W = H_{TTFA} - H_{Current} \qquad (17)$$

$$H_{TTFA} = H_{Current} \cdot \frac{D_{Current} - D_W}{D_{TTFA} - D_W} \qquad (18)$$

$$D_{Current} = \frac{1}{h_{ms} - h_{ft}} \cdot \int_{h_{ft}}^{h_{ms}} D(h) \cdot dh \quad (h_{ms} - h_{ft} = H_{Current}) \qquad (19)$$

$$D_{TTFA} = \frac{1}{h_{mst} - 0} \cdot \int_{0}^{h_{mst}} D(h) \cdot dh \quad (h_{mst} - 0 = H_{TTFA}) \qquad (20)$$

$$D(h) = -0.00000003 \cdot h^2 + 0.00034 \cdot h + 1.6019 \quad (R^2 = 0.6149) \qquad (21)$$

where H_{TTFA} is the thickness of the sedimentary interval from the mudstone caprock to the top of the fault at the termination time of fault activity (TTFA), m; D_{TTFA} is the average density of the sedimentary interval from the mudstone caprock to the top of the fault at the TTFA, g/cm^3; $H_{Current}$ is the thickness of the sedimentary interval from the mudstone caprock to the top of the fault on the present day, m; $D_{Current}$ is the average density of the sedimentary interval from the mudstone caprock to the top of the fault on the present day, g/cm^3; H_W is the thickness of water discharged due to compaction after TTFA, m; D_W is the density of formation water, 1.03 g/cm^3; h_{ms} is the current burial depth of mudstone caprock, m; h_{ft} is the burial depth at the top of the fault, m; $D(h)$ is the function of bulk density that varies with burial depth; h is the burial depth, m; and h_{mst} represents the paleoburial depth of the mudstone caprock at the TTFA, m.

3.3. Quantitative evaluation of the sealing capability of mudstone caprock

Since mudstone in different deformation stages has distinct deformation mechanisms, the evaluation of sealing capacity should be characterized from different aspects. In this article, the method of caprock juxtaposition thickness (CJT) and shale smear factor (SSF) are adopted to evaluate the sealing capacity of brittle and brittle-ductile mudstone caprocks, respectively.

3.3.1. Quantitative evaluation of the sealing capability of brittle mudstone

With the increase in shear deformation caused by fault sliding, fractures occur in the brittle mudstone and gradually interconnect to form networks, resulting in greater permeability and less sealing capability (Anderson, 1994; Bolton and Maltman, 1998; Ingram and Urai, 1999; Jin et al., 2014) (Fig. 6a). Under this condition, the vertical permeability of mudstone caprock is predominantly affected by the two major factors of fault displacement (or throw) and mudstone thickness. Generally, increasing fault displacement will lead to an increase in strain and more fracture development, while a thin mudstone layer is more conducive to the generation of an interconnected fracture network (Fu et al., 2019). All these factors have contributed to the reduction of caprock-sealing capability and the occurrence of hydrocarbon leakage. For this reason, the juxtaposed thickness of the caprock after faulting (CJT) (Lü et al., 2007) is used to quantitatively characterize the vertical connectivity of the fracture (Fig. 6d) and thus to evaluate the top sealing ability of the mudstone caprock. The CJT is defined as the difference between the thickness of the caprock and the fault throw, as expressed in Equation (22).

$$CJT = MT - T = MT - Dsin\alpha \qquad (22)$$

where CJT is the caprock juxtaposition thickness (m), MT is the thickness of the mudstone (m), T is the fault throw (m), D is the fault displacement (m) and α is the dip angle of the fault (°). The values of MT, T, D and α can be obtained from seismic interpretation profiles.

3.3.2. Quantitative evaluation of the sealing capability of brittle-ductile mudstone

Mudstone subjected to the brittle-ductile stage is difficult to cut through by faults. Since mudstone has obvious competence compared with brittle lithologies (e.g., sandstone), faults are preferentially generated in brittle strata and present vertical segmented growth (Lehner and Pilaar, 1997; Sperrevik et al., 2000; Rykkelid and Fossen, 2002; Doughty, 2003) (Fig. 6b). As a result, plastic mudstone will be dragged into the fault zone during the faulting processes and form a
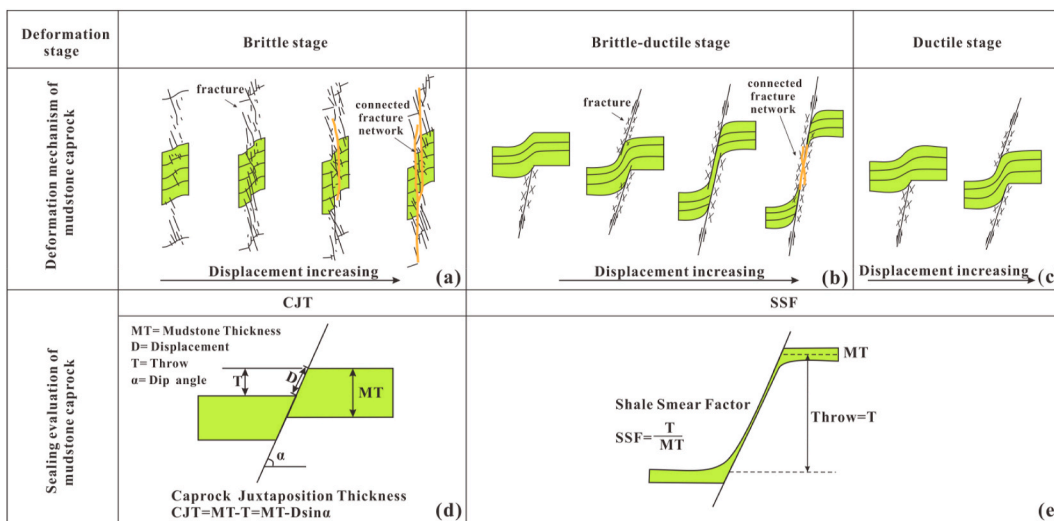
Fig. 6. Deformation mechanisms and sealing quantitative evaluation of mudstone caprock. (a), (b), and (c) show the brittle, brittle-ductile and ductile deformation mechanisms of mudstone caprock controlled by fault activity, respectively (after Fossen, 2010; Fu et al., 2019). (d) The method of caprock juxtaposition thickness (CJT) for brittle rock (Lü et al., 2007). (e) The method of the shale smear factor (SSF) for brittle-ductile rock (Lindsay et al., 1993).
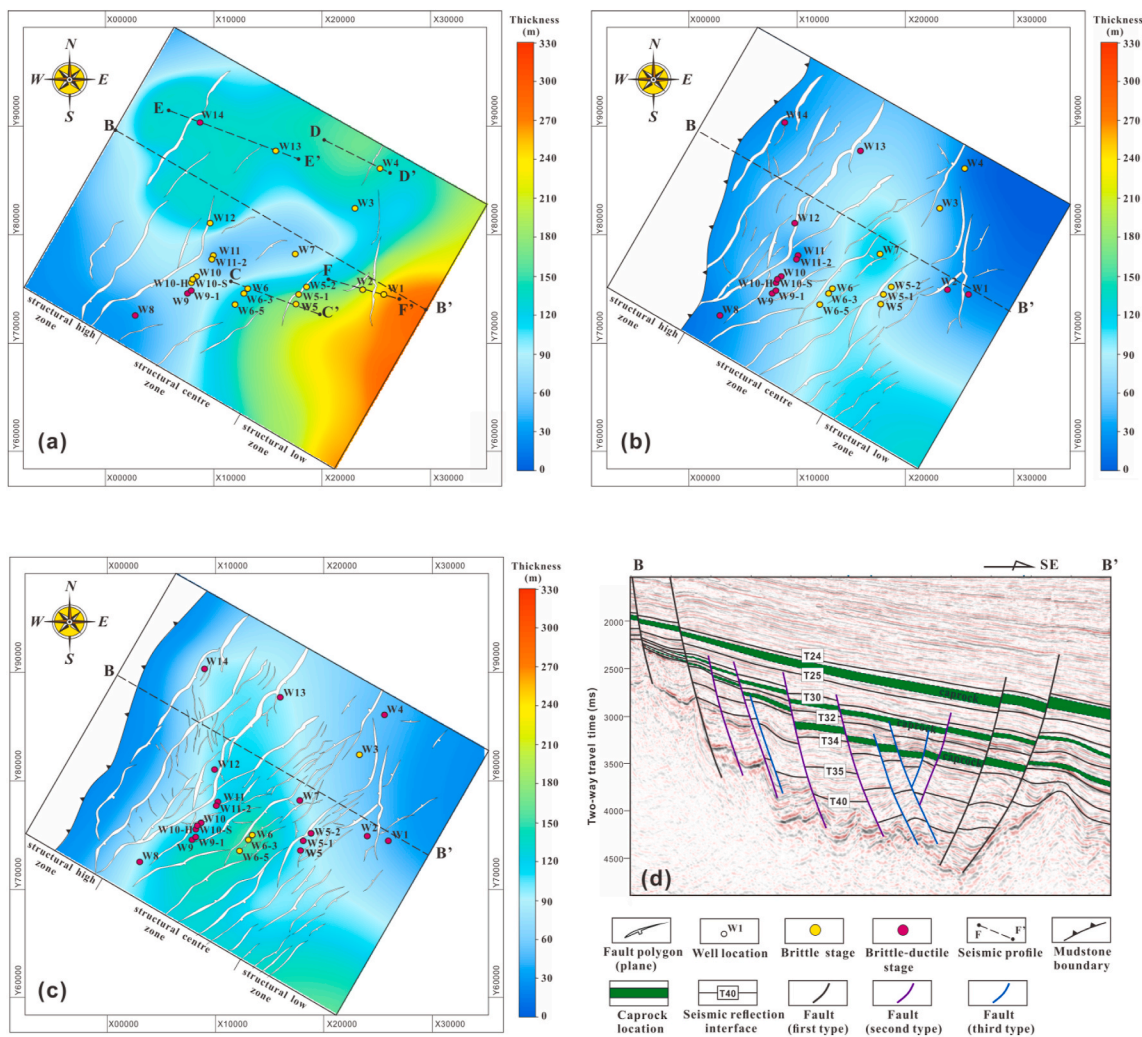

Fig. 7. (a), (b), and (c) show the mudstone thickness and normal fault distribution of the E_3h_1, E_2p_1, and E_2p_3 caprocks, respectively. The brittle-ductile reconstruction results of mudstone located in different well positions are represented by yellow dots (brittle stage) and red dots (brittle-ductile stage). (d) Distribution characteristics of mudstone caprocks and faults on the BB′ profile; see Fig. 7a for the location. (For interpretation of the references to colour in this figure legend, the reader is referred to the Web version of this article.)

typical shale shear zone. (Doughty, 2003; Davatzes and Aydin, 2005; Cuisiat and Skurtveit, 2010; Wang et al., 2020). Previous studies have proven that continuous shale/mudstone smears can effectively prevent upward leakage of hydrocarbons (Lindsay et al., 1993; Yielding et al., 1997; Fulljames et al., 1997; Childs et al., 2007); therefore, caprock sealing can be evaluated by analyzing the shale smear continuity. The continuity of shale smears predominantly depends on the ratio of fault throw and mudstone thickness, which can be quantitatively determined by the shale smear factor (SSF) (Lindsay et al., 1993), as written in Equation (23).

$$SSF = \frac{Fault\ throw}{Mudstone\ layer\ thickness} \qquad (23)$$

where the SSF is dimensionless and the fault throw and mudstone layer thickness are in meters. The fault throw data can be measured from the seismic interpretation profiles, and the mudstone layer thickness can be interpreted by a combination of logging curves and seismic attributes. Therefore, by combining the two quantitative methods, CJT and SSF, the sealing capability of mudstone caprock with different brittleness-ductility can be systematically evaluated.

4. Results and discussion

4.1. Spatial distribution of normal faults and mudstone caprocks in the K gasfield

Combining drilling data, geophysical logging and seismic interpretation, the thickness of the three major mudstone caprocks is obtained, as shown in Fig. 7. For the shallowest buried E_3h_1 caprock, thick mudstone with a thickness of more than 150 m is widely distributed to the south of well W5 and east of well W12, showing a decreasing trend from the structurally lower position to the structurally higher position (Fig. 7a). However, the E_2p_1 caprock has a relatively thin thickness distribution, mostly 30–100 m, except for mudstones with a thickness of 100–120 m distributed in the southern part of well W6 (Fig. 7b). In addition, the E_2p_3 caprock, whose thickness is mainly 100–180 m, shows a similar changing trend to E_2p_1 (Fig. 7c). Overall, these three caprocks have a thinner thickness in the structurally higher position and the eastern part of well W2, and the thickness of E_3h_1 is generally thicker than that of E_2p_1 and E_2p_3.

The plane polygons and vertical geometry of the faults interpreted from 3D seismic volume are also shown in Fig. 7. The faults in the study area can be generally divided into three categories according to the topmost position of the fault in the spatial content (Fig. 7d). The first type of fault has a terminal position located in or above the E_3h_1 caprock, and the corresponding fault activity could have caused deformation in the E_3h_1, E_2p_1, and E_2p_3 caprocks. However, the topmost position of the second type of fault is located between the E_3h_1 and E_2p_1 caprocks, and its movement only affected the continuity of the E_2p_1 and E_2p_3 caprocks. Furthermore, the third type of fault with a top end position below the E_2p_1 caprock only had an effect on the sealing capacity of the E_2p_3 caprock. The increasing number of the first, second, and third types of faults indicates that the E_2p_1 and E_2p_3 caprocks experienced more shear deformation caused by fault activity compared with the E_3h_1 caprock deposited later (Fig. 7a–c). However, the sealing capability of caprock controlled by faults needs to be further analyzed in conjunction with the brittle-ductile properties of mudstone.

4.2. Brittle-ductile characteristics of mudstone caprock in the K gas field

4.2.1. Critical conditions for the mudstone brittle-ductile transformation

The caprocks distributed in the E_3h_1, E_2p_1 and E_2p_3 formations are dominated by gray mudstone, and the shale volume content (V_{sh}) of the gray mudstone is generally greater than 70%. To obtain more evaluation data, in addition to the mudstone acting as caprock, noncaprock

mudstone with greater than 70% was also selected to establish the evaluation model of brittle-ductile transformation (Fig. 8a). In this way, quantitative calculations were performed on 5 wells for which all relevant logging data were available, and the fitted Mohr-Coulomb fracture envelope was combined with Byerlee friction law and Goetze's criterion to determine the critical conditions for mudstone brittle-ductile transformation. The critical confining pressures for mudstone transformation from the brittle to brittle-ductile stage and from the brittle-ductile to ductile stage are 19 MPa and 95 MPa, respectively (Fig. 8b). As the effective confining pressure is a function of depth, the critical confining pressure can be approximately equal to the critical burial depths of 2071.0 m and 7680.0 m, respectively. Therefore, the E_3h_1, E_2p_1 and E_2p_2 mudstone caprocks with a current burial depth of 2500–4800 m are all in the brittle-ductile (semibrittle) stage. However, due to the difference in paleoburial depth, the mudstone caprock may be in a different deformation stage at the termination time of fault activity (TTFA).

4.2.2. Brittle-ductile characteristics of mudstone caprock at the TTFA

The quantitative method for determining the paleoburial depth was applied to restore the brittle-ductile stage of the caprock at the termination time of fault activity (TTFA), and we calculated this for the mudstone caprocks in the Upper Huagang and Upper and Lower Pinghu Formations, and the results are shown in Table 1. Comparing the reconstructed burial depth with the critical burial depth for the brittle-ductile transformation, the shallowly buried E_3h_1 caprock was generally in the brittle stage at the TTFA, except for the mudstone that had entered the brittle-ductile stage in wells W8, W9, W9-1 and W14 (Fig. 7a). The reconstruction results show that the E_2p_1 caprock had two main stages of brittleness and brittleness-ductility (semibrittleness) at the TTFA. In detail, the mudstone caprocks in the brittle stage are concentrated in the central areas around wells W5 and W6, while the mudstone caprocks entering the brittle-ductile stage are mainly located around well W2 and the northern part of well W9 (Fig. 7b). However, for the deepest buried E_2p_3 caprock at the TTFA, the mudstone was generally in the same brittle-ductile stage as the current mudstone, except for the mudstone located near well W6 (Fig. 7c). Therefore, from the perspective of rock shear deformation, the E_2p_3 mudstone caprock dominated by brittle-ductile deformation was more likely to form a shale smear zone to prevent the vertical leakage of hydrocarbons unless it lost continuity. In contrast, the E_3h_1 mudstone caprock dominated by brittle deformation was more likely to form a connected fracture network under the sliding of faults, resulting in reduced sealing capacity and hydrocarbon leakage. Nevertheless, the sealing capacity of mudstone caprock still needs to be comprehensively analyzed in combination with fault displacement and mudstone thickness.

4.3. Caprock-sealing capability and hydrocarbon accumulation response

Spatially continuous mudstone caprock serves as an effective top barrier to prevent the vertical leakage of hydrocarbons. However, fault activity will destroy the integrity of the mudstone caprock and increase the vertical permeability, thereby reducing its ability to seal hydrocarbons. Considering the deformation mechanisms of mudstone in different stages, the sealing properties of brittle and brittle-ductile mudstones were quantitatively evaluated by the caprock juxtaposition thickness (CJT) and shale smear factor (SSF), respectively. Furthermore, combined with the hydrocarbon accumulation and distribution in the K gasfield, two critical thresholds were determined to separate the sealing and nonsealing mudstone caprocks and finally revealing the hydrocarbon accumulation response controlled by mudstone caprock sealing.

4.3.1. Relationship between caprock juxtaposition thickness (CJT) and vertical hydrocarbon accumulation

The caprock juxtaposition thickness (CJT) can quantitatively describe the destruction of fault activity on the integrity of brittle mudstone caprock. When the fault throw is greater than the caprock
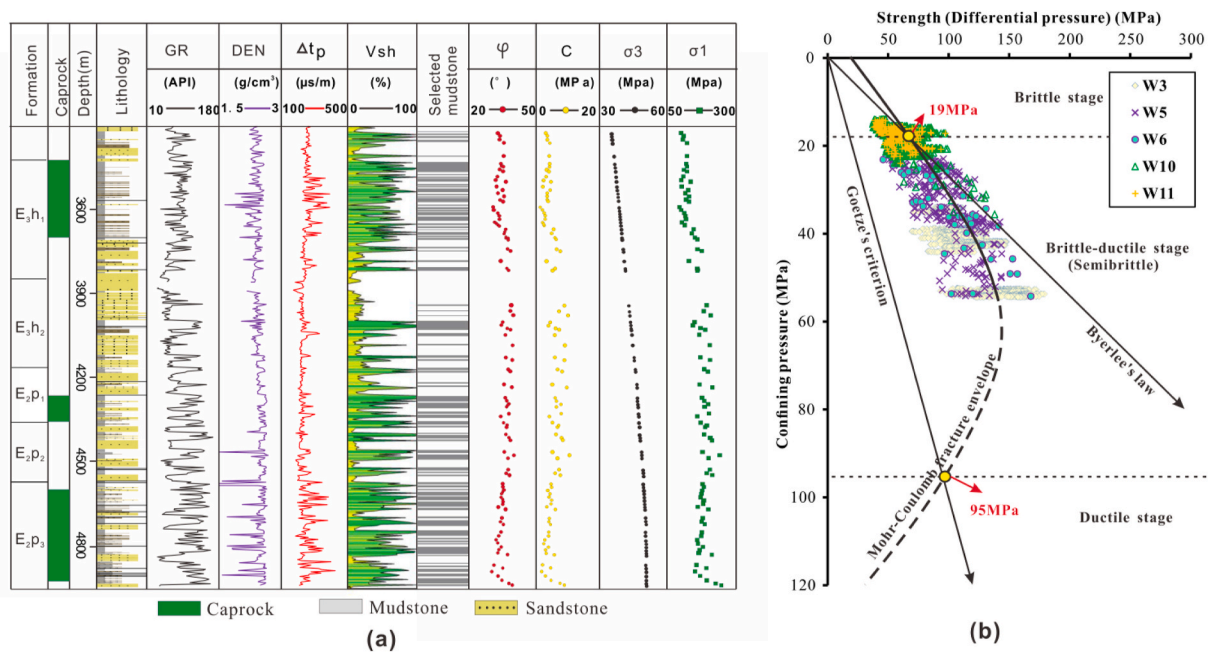
Fig. 8. (a) An example of using geophysical logging data to estimate the mechanical properties of mudstone in well W5. **GR** is the gamma ray, **DEN** is the compensated density, Δt_p is the P-wave travel time, V_{sh} is the shale volume content, ϕ is the rock internal friction angle, C is the cohesion of rock, $\sigma 3$ is the minimum principal stress, and $\sigma 1$ is the maximum principal stress; (b) Quantitative model to determine the critical effective confining pressure of the brittle-ductile transformation of mudstone caprocks in the K gasfield in the Xihu Depression. The black dashed line represents the forecast tendency of the Mohr-Coulomb fracture envelope.

thickness, the caprock is completely broken by the fault and loses its sealing ability. Conversely, the caprock layer will maintain continuity in the lateral direction when the fault throw is less than the caprock thickness, thus sealing a certain height of the hydrocarbon column. However, in general, vertical leakage of hydrocarbons will occur when the juxtaposition thickness after faulting is less than a critical value.

In the K gasfield in the Xihu Depression, CJT was calculated for mudstone caprock in the brittle deformation stage at the TTFA. The mudstone caprocks in E_3h_1 and E_2p_1 are the regional caprocks covering the upper and middle petroleum systems in the K gasfield, respectively. Although the main hydrocarbon charging time (Pliocene) determined from fluid inclusions (Shan et al., 2015; Su et al., 2015) was significantly later than the duration of fault activity (Paleogene) in the study area (Wang et al., 2021), the integrity of the mudstone caprock has been destroyed to varying degrees by fault activity and allowed some hydrocarbons to pass through the caprock. Generally, hydrocarbon occurrences above and below the caprock can provide an indication of the effectiveness of caprock sealing. The hydrocarbon accumulations or shows above the regional caprock indicate possible vertical leakage, while the concentrated accumulation of hydrocarbons below the caprock demonstrates the effective top seal of the cap layer. Statistics on the CJT of mudstone caprocks reveal that the E_3h_1 caprock has a significantly larger CJT value than the E_2p_1 caprock, indicating a stronger vertical sealing ability (Fig. 9). Furthermore, the threshold value of CJT for caprock sealing can be approximately determined by the relationship between the evaluated CJT and the corresponding vertical hydrocarbon distribution. According to the occurrence of oil and gas matching the caprock (Fig. 9), none of the mudstone caprocks with a CJT value equal to or greater than 56.1 m has experienced hydrocarbon vertical leakage, while most mudstone caprocks with a CJT value less than 56.1 m have contributed to the vertical migration of hydrocarbons. Therefore, the threshold value of CJT (abbreviated as $CJT_{threshold}$) for caprock sealing in the K gasfield can be approximately defined as 56.1 m, which represents the statistical law that vertical leakage of hydrocarbons will occur when the CJT value of caprock is less than 56.1 m.

Sections CC′ and DD′ are taken as examples to illustrate the effect of

CJT on hydrocarbon migration and accumulation (Fig. 10). In profile CC′, the hydrocarbons generated from WSS migrated laterally along the SE-NW direction, and the vertical distribution of hydrocarbons varied with the CJT value of the caprock (Fig. 10b). The E_2p_1 caprock has a CJT value less than 56.1 m at well W5, resulting in obvious vertical leakage of hydrocarbons. However, the CJT value of the E_2p_1 caprock at well W6 is greater than the threshold value; therefore, the hydrocarbons are all sealed below the caprock. In addition, the E_3h_1 caprock has a CJT value significantly greater than the threshold value (56.1 m) and generally acts as an effective top seal for the upper petroleum system. However, the E_2p_1 caprock in the DD' profile completely lost its continuity due to the large fault displacement, resulting in a large scale of hydrocarbon leakage (Fig. 10d). All these results illustrate the control of the juxtaposition thickness of brittle mudstone caprock on hydrocarbon migration and accumulation.

4.3.2. Relationship between the shale smear factor (SSF) and vertical hydrocarbon accumulation

The continuity of mudstone caprock in the brittle-ductile deformation stage can be quantitatively assessed by the shale smear factor (SSF). On the whole, mudstone caprock is vertically sealed when shale smears in the fault zone maintains continuity. However, once the SSF exceeds a critical threshold, the continuity of shale smears will be destroyed, leading to upward migration of hydrocarbons. Additionally, the threshold value of the SSF on shale smear continuity generally varies with the scale of the fault. Small faults with a displacement less than 15 m remain continuous when the SSF changes from 1 to 50 (Faerseth, 2006), while large-scale faults whose displacements are greater than 15 m usually have a threshold value of a SSF between 4 and 8 (Yielding, 2002; Doughty, 2003; Faerseth, 2006). For the specific study area, the SSF threshold for shale smear continuity can be determined in detail based on the hydrocarbon occurrences above and below the caprock.

At the termination time of fault activity, the mudstone caprocks of E_2p_1 and E_2p_3 in the K gas field were generally in the brittle-ductile deformation stage, which serve as the top seals for the middle and lower petroleum systems, respectively. According to the SSF calculation

Table 1

Reconstruction results of the brittle-ductile stage of the mudstone caprock at the termination time of fault activity (TTFA).

Mudstone caprock	Well	h_{ms}	h_{ft}	$H_{Current}$	$D_{Current}$	h_{mst}	Brittle-ductile stage		
							BDTH	present day	TTFA
E_3h_1	W1	3797.1	2790.8	1006.3	2.4	1467.0	2071.0	brittle-ductile	brittle
E_3h_1	W2	3758.5	2535.0	1223.5	2.4	1727.6	2071.0	brittle-ductile	brittle
E_3h_1	W3	3625.2	3288.0	337.2	2.4	527.9	2071.0	brittle-ductile	brittle
E_3h_1	W4	3628.8	2913.2	715.6	2.4	1066.0	2071.0	brittle-ductile	brittle
E_3h_1	W5	3600.3	3272.1	328.2	2.4	513.2	2071.0	brittle-ductile	brittle
E_3h_1	W5-1	3621.0	3283.2	337.8	2.4	528.5	2071.0	brittle-ductile	brittle
E_3h_1	W5-2	3615.1	3264.2	350.9	2.4	547.8	2071.0	brittle-ductile	brittle
E_3h_1	W6	3238.2	2944.0	294.2	2.4	445.7	2071.0	brittle-ductile	brittle
E_3h_1	W6-3	3234.5	2936.3	298.2	2.4	451.3	2071.0	brittle-ductile	brittle
E_3h_1	W6-5	3230.4	2919.3	311.1	2.4	469.7	2071.0	brittle-ductile	brittle
E_3h_1	W7	3506.7	2699.9	806.8	2.4	1172.7	2071.0	brittle-ductile	brittle
E_3h_1	W8	2668.3	708.9	1959.5	2.1	2112.2	2071.0	brittle-ductile	brittle-ductile
E_3h_1	W9	2929.0	1019.5	1909.5	2.1	2181.0	2071.0	brittle-ductile	brittle-ductile
E_3h_1	W9-1	2925.8	1017.0	1908.8	2.1	2179.2	2071.0	brittle-ductile	brittle-ductile
E_3h_1	W10	2954.2	1475.5	1478.7	2.2	1816.0	2071.0	brittle-ductile	brittle
E_3h_1	W10–S	2950.6	1486.2	1464.4	2.2	1801.4	2071.0	brittle-ductile	brittle
E_3h_1	W10–H	2956.1	1471.5	1484.6	2.2	1822.2	2071.0	brittle-ductile	brittle
E_3h_1	W11	3116.6	1747.0	1369.6	2.2	1752.5	2071.0	brittle-ductile	brittle
E_3h_1	W11-2	3110.0	1753.9	1356.1	2.2	1737.0	2071.0	brittle-ductile	brittle
E_3h_1	W12	3029.2	1885.8	1143.4	2.2	1494.0	2071.0	brittle-ductile	brittle
E_3h_1	W13	3300.4	2314.1	986.3	2.3	1366.3	2071.0	brittle-ductile	brittle
E_3h_1	W14	2665.1	469.3	2195.8	2.0	2267.1	2071.0	brittle-ductile	brittle-ductile
E_2p_1	W1	4398.8	2790.8	1608.0	2.4	2292.6	2071.0	brittle-ductile	brittle-ductile
E_2p_1	W2	4460.6	2535.0	1925.6	2.4	2656.5	2071.0	brittle-ductile	brittle-ductile
E_2p_1	W3	4220.9	3288.0	932.9	2.4	1422.3	2071.0	brittle-ductile	brittle
E_2p_1	W4	4262.1	2913.2	1348.9	2.4	1962.4	2071.0	brittle-ductile	brittle
E_2p_1	W5	4290.2	3272.1	1018.1	2.5	1544.2	2071.0	brittle-ductile	brittle
E_2p_1	W5-1	4292.2	3283.2	1009.0	2.5	1532.3	2071.0	brittle-ductile	brittle
E_2p_1	W5-2	4280.5	3264.2	1016.3	2.4	1540.7	2071.0	brittle-ductile	brittle
E_2p_1	W6	4013.5	2944.0	1069.5	2.4	1577.3	2071.0	brittle-ductile	brittle
E_2p_1	W6-3	4010.0	2936.3	1073.7	2.4	1582.2	2071.0	brittle-ductile	brittle
E_2p_1	W6-5	4007.6	2919.3	1088.3	2.4	1600.4	2071.0	brittle-ductile	brittle
E_2p_1	W7	4153.5	2699.9	1453.6	2.4	2069.1	2071.0	brittle-ductile	brittle
E_2p_1	W8	3028.2	708.9	2319.4	2.1	2519.7	2071.0	brittle-ductile	brittle-ductile
E_2p_1	W9	3406.6	1019.5	2387.1	2.2	2736.1	2071.0	brittle-ductile	brittle-ductile
E_2p_1	W9-1	3401.1	1017.0	2384.1	2.2	2731.6	2071.0	brittle-ductile	brittle-ductile
E_2p_1	W10	3432.8	1475.5	1957.3	2.2	2402.8	2071.0	brittle-ductile	brittle-ductile
E_2p_1	W10–S	3429.5	1486.2	1943.3	2.2	2389.4	2071.0	brittle-ductile	brittle-ductile
E_2p_1	W10–H	3425.9	1471.5	1954.4	2.2	2397.9	2071.0	brittle-ductile	brittle-ductile
E_2p_1	W11	3520.7	1747.0	1773.7	2.3	2262.1	2071.0	brittle-ductile	brittle-ductile
E_2p_1	W11-2	3512.4	1753.9	1758.5	2.3	2245.2	2071.0	brittle-ductile	brittle-ductile
E_2p_1	W12	3511.2	1885.8	1625.4	2.3	2114.1	2071.0	brittle-ductile	brittle-ductile
E_2p_1	W13	3934.1	2314.1	1620.0	2.4	2212.0	2071.0	brittle-ductile	brittle-ductile
E_2p_1	W14	3031.0	469.3	2561.7	2.1	2670.5	2071.0	brittle-ductile	brittle-ductile
E_2p_3	W1	4450.3	2790.8	1659.5	2.4	2361.1	2071.0	brittle-ductile	brittle-ductile
E_2p_3	W2	4620.8	2535.0	2085.8	2.4	2859.9	2071.0	brittle-ductile	brittle-ductile
E_2p_3	W3	4668.9	3288.0	1380.9	2.5	2060.1	2071.0	brittle-ductile	brittle
E_2p_3	W4	4600.1	2913.2	1686.9	2.4	2419.2	2071.0	brittle-ductile	brittle-ductile
E_2p_3	W5	4800.7	3272.1	1528.6	2.5	2261.2	2071.0	brittle-ductile	brittle-ductile
E_2p_3	W5-1	4810.1	3283.2	1526.9	2.5	2260.4	2071.0	brittle-ductile	brittle-ductile
E_2p_3	W5-2	4785.6	3264.2	1521.4	2.5	2250.3	2071.0	brittle-ductile	brittle-ductile
E_2p_3	W6	4423.4	2944.0	1479.4	2.4	2045.6	2071.0	brittle-ductile	brittle
E_2p_3	W6-3	4419.5	2936.3	1483.2	2.4	2049.6	2071.0	brittle-ductile	brittle
E_2p_3	W6-5	4415.0	2919.3	1495.7	2.4	2063.7	2071.0	brittle-ductile	brittle
E_2p_3	W7	4517.2	2699.9	1817.3	2.4	2551.1	2071.0	brittle-ductile	brittle-ductile
E_2p_3	W8	3326.0	708.9	2617.2	2.1	2853.7	2071.0	brittle-ductile	brittle-ductile
E_2p_3	W9	3680.1	1019.5	2660.6	2.2	3048.4	2071.0	brittle-ductile	brittle-ductile
E_2p_3	W9-1	3678.4	1017.0	2661.4	2.2	3048.2	2071.0	brittle-ductile	brittle-ductile
E_2p_3	W10	3679.4	1475.5	2203.9	2.2	2699.8	2071.0	brittle-ductile	brittle-ductile
E_2p_3	W10–S	3675.8	1486.2	2189.6	2.2	2686.5	2071.0	brittle-ductile	brittle-ductile
E_2p_3	W10–H	3671.2	1471.5	2199.7	2.2	2693.4	2071.0	brittle-ductile	brittle-ductile
E_2p_3	W11	3866.0	1747.0	2119.0	2.3	2688.4	2071.0	brittle-ductile	brittle-ductile
E_2p_3	W11-2	3859.3	1753.9	2105.4	2.3	2674.0	2071.0	brittle-ductile	brittle-ductile
E_2p_3	W12	3949.7	1885.8	2063.9	2.3	2663.5	2071.0	brittle-ductile	brittle-ductile
E_2p_3	W13	4415.0	2314.1	2100.9	2.4	2826.5	2071.0	brittle-ductile	brittle-ductile
E_2p_3	W14	3200.5	469.3	2731.2	2.1	2856.0	2071.0	brittle-ductile	brittle-ductile

Note: h_{ms}: Current burial depth of mudstone caprock, m; h_{ft}: burial depth at the top of the fault, m; $H_{Current}$: thickness of the stratigraphic interval from the central mudstone caprock to the top of the fault on the present day, m; $D_{Current}$: current average density of the stratigraphic interval from the central mudstone caprock to the top of the fault, g/cm^3; h_{mst}: paleoburial depth of the mudstone caprock at the TTFA, m; and BDTH: critical depth transformation from the brittle to brittle-ductile stage.
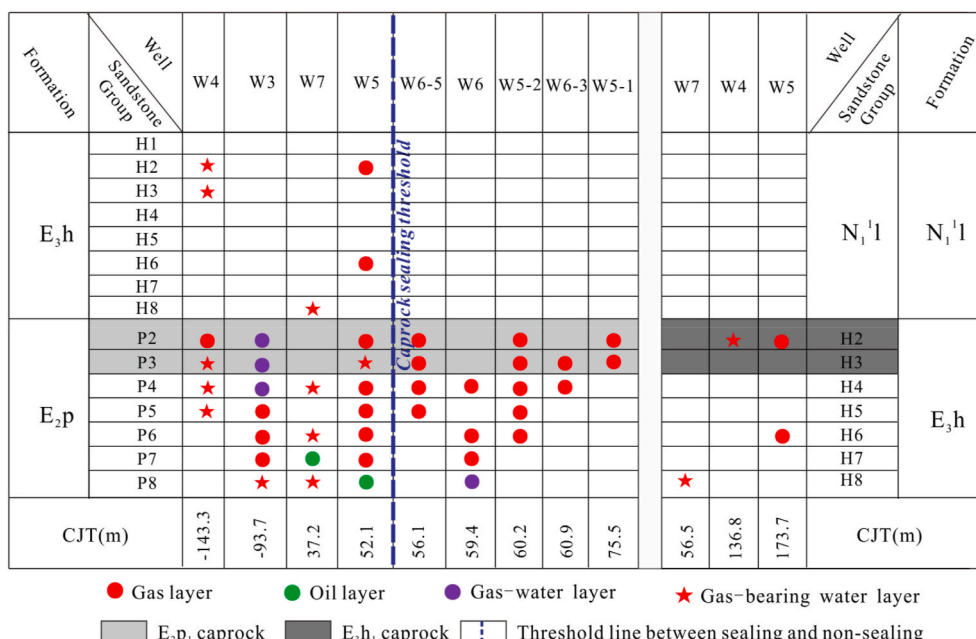
Fig. 9. Determination of the threshold of juxtaposition thickness of mudstone caprock in the K gasfield in the Xihu depression.

of the brittle-ductile mudstone and the corresponding oil and gas occurrences (Fig. 11), the critical threshold of shale smear continuity can be determined to be 3.0. Thus, mudstone caprock with an SSF greater than 3.0 usually loses its continuity, thereby resulting in vertical leakage of hydrocarbons. Profiles EE′ and FF′ are taken as cases to illustrate the effect of the SSF on hydrocarbon migration and accumulation (Fig. 12a and Fig. 12b). For the EE′ profile in the structural high zone, hydrocarbon accumulations mainly came from the lateral charging of hydrocarbons generated by the mature source rock in the WSS. The E_2p_1 caprock around well W13 was in the brittle-ductile deformation stage at the TTFA, and mudstone with a continuous shale smear (SSF<3.0) effectively prevented the upward migration of hydrocarbons under the caprock (Fig. 12b). However, when the laterally migrated hydrocarbon encountered the E_2p_1 caprock with an SSF greater than 3.0 near well W14, the hydrocarbon in the middle petroleum system had leaked to the upper petroleum system. For the FF′ profile in the structural low zone, the SSF value of the E_2p_1 mudstone caprock around wells W1 and W2 is greater than 3.0, thus resulting in a large scale of hydrocarbon migration through the caprock and accumulation in the reservoir within the upper petroleum system (Fig. 12c and d).

4.3.3. Comparison between the current and TTFA caprock-sealing evaluation

In terms of current mechanical properties, the sealing capability of E_3h_1, E_2p_1 and E_2p_3 caprocks during the brittle-ductile (semibrittle) stage should be quantitatively evaluated by the SSF. However, the reconstructed paleodepths show that most mudstones were still in the brittle stage at the TTFA, especially the E_3h_1 and E_2p_1 caprocks. Therefore, errors may occur when the SSF method is incorrectly applied to evaluate the caprock that is undergoing brittle deformation, and this deviation in the sealing evaluation will directly affect the judgment on the effectiveness of the caprock.

Theoretically, when the SSF and CJT methods are applied to assess the sealing capability of the same caprock, the following three situations will appear due to disparities in fault throw (T) and mudstone thickness (MT) (Fig. 13). In the first case, the fault throw and mudstone thickness satisfy the relationship of CJT > $CJT_{threshold}$ (the threshold of juxtaposition thickness for caprock sealing) and SSF<1- $CJT_{threshold}$/MT, and the difference in brittleness-ductility will not contribute to changes in the evaluation results of caprock sealing. Taking the E_2p_1 caprock near

well W6 as an example, the mudstone caprock at this location is currently in the brittle-ductile (semibrittle) stage but was in the brittle stage at the TTFA. The SSF and CJT results matching the current and TTFA situation all indicate that it is an effective top seal. However, in the second case where the fault throw and mudstone thickness meet the relationship of (1-$SSF_{threshold}$)MT < CJT < $CJT_{threshold}$ and 1-$CJT_{threshold}$/MT < SSF < $SSF_{threshold}$ (the threshold of shale smear factor for caprock sealing), the evaluation results from the different methods will show disparities. Taking the E_2p_1 caprock around well W5 as an example, the mudstone is also currently in the brittle-ductile (semibrittle) stage but was in the brittle stage at the TTFA. However, the SSF evaluation based on the current brittle-ductile stage indicates the effective sealing of the caprock, whereas the CJT evaluation corresponding to the TTFA implies the presence of vertical hydrocarbon leakage. The hydrocarbon occurrence further confirms that the CJT evaluation matching the brittle deformation of mudstone at the TTFA reveals the caprock sealing more accurately. Nevertheless, when the fault throw and mudstone thickness satisfy the third conditions of relationships CJT<(1- $SSF_{threshold}$)MT and SSF > $SSF_{threshold}$, the evaluation results of these two methods are again consistent, and the E_2p_1 caprock around well W4 supports this interpretation. As shown in Fig. 13, whether brittle or brittle-ductile mudstone is present, a large fault throw will cause it to lose continuity (or integrity) and result in vertical leakage of hydrocarbons. However, in general, the brittle-ductile reconstruction and corresponding sealing evaluation at the TTFA can describe the effectiveness of the mudstone caprock more accurately.

4.3.4. Hydrocarbon accumulation model for the control of caprock sealing

Due to the distinction in the brittle-ductile stages, three major mudstone caprocks, E_3h_1, E_2p_1 and E_2p_3, in the K gasfield have undergone varying shear deformations at the TTFA. Therefore, the caprock sealing controlled by the fault throw and mudstone thickness has further affected hydrocarbon accumulation and distribution, and the model can be summarized in Fig. 14.

With respect to the E_2p_3 mudstone caprock with a thickness of mostly 100–180 m, the typical shale smear zone was formed at the TTFA due to its brittle-ductile deformation, and the shear deformation induced by fault activity failed to break the continuity of mudstone, except for that in well W1 in the structural low zone. Although the E_2p_1 mudstone
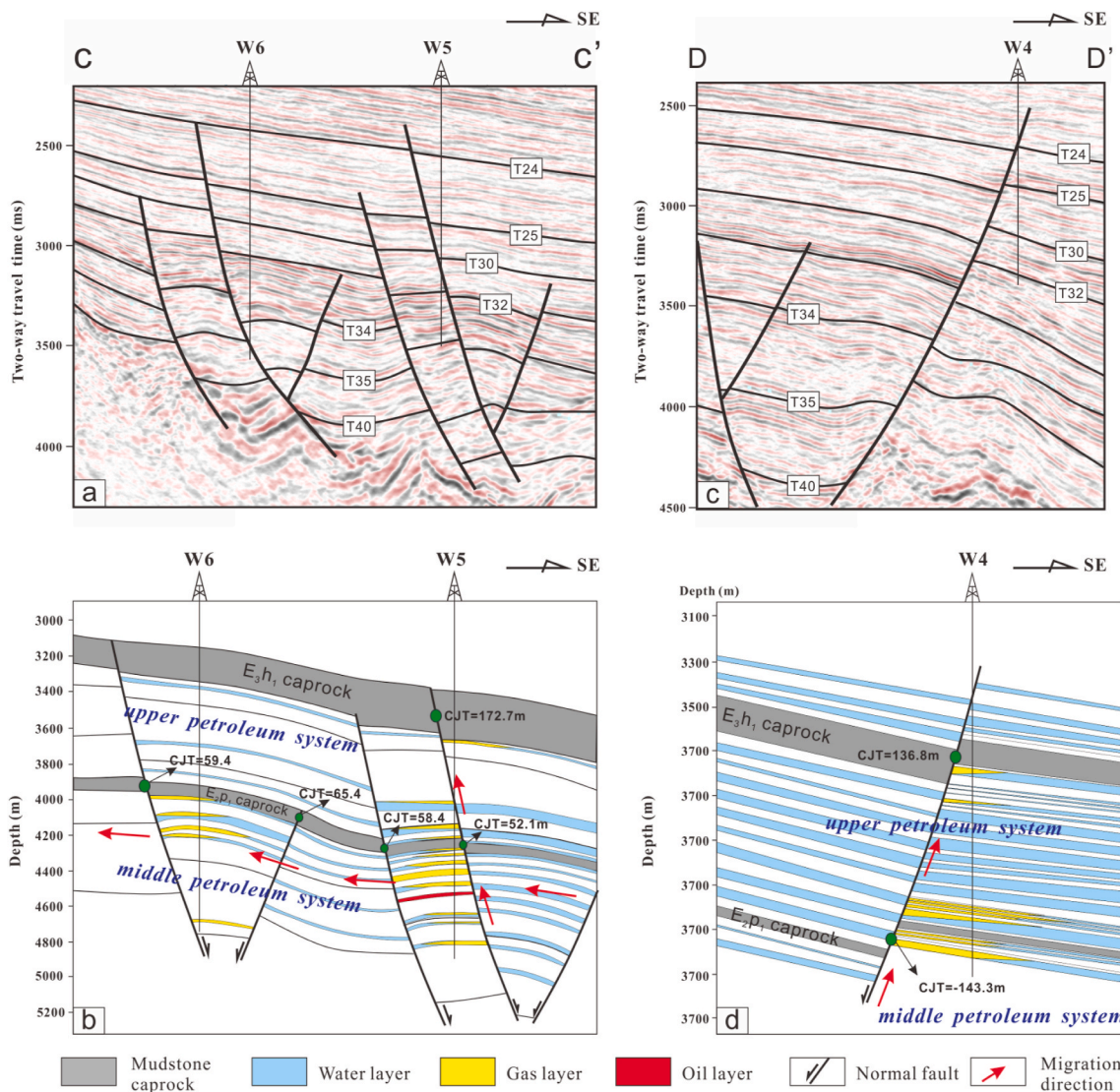
Fig. 10. (a) and (b) show the normal faults, mudstone caprocks, and corresponding hydrocarbon distribution characteristics in the CC′ profile. (c) and (d) show the normal faults, mudstone caprocks, and corresponding hydrocarbon distribution characteristics in the DD′ profile. See Fig. 7a for locations.
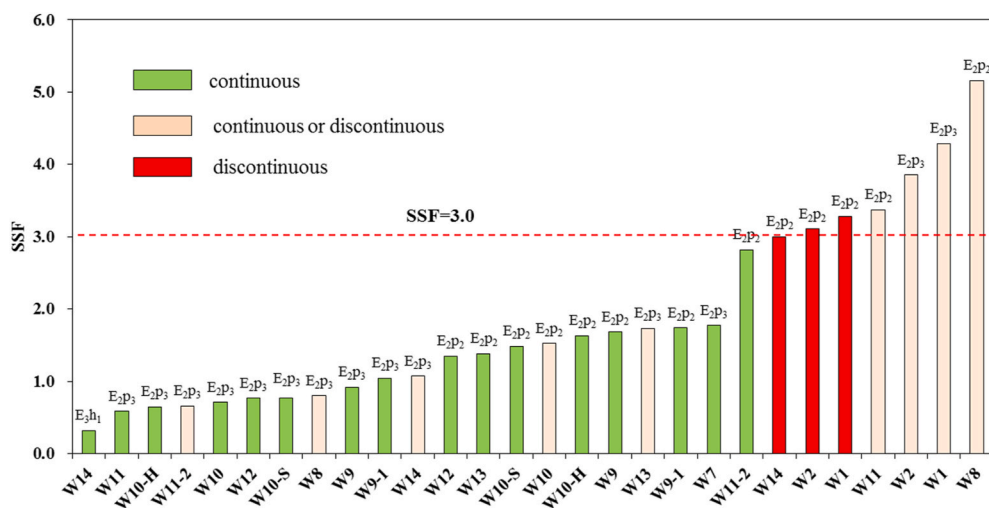

Fig. 11. Determination of the threshold of the shale smear factor of mudstone caprock in the K gasfield in the Xihu depression. The continuity of the cap layer is judged by the hydrocarbon occurrences above and below the cap layer. The hydrocarbon shows above the regional caprock usually indicate the vertical leakage caused by the discontinuous caprock, while the concentrated accumulation of hydrocarbons below the caprock demonstrates the effective top seal of the continuous cap layer. However, when the continuity cannot be effectively determined due to the influence of lateral migration, the cap layer is defined as a "continuous or discontinuous" state.
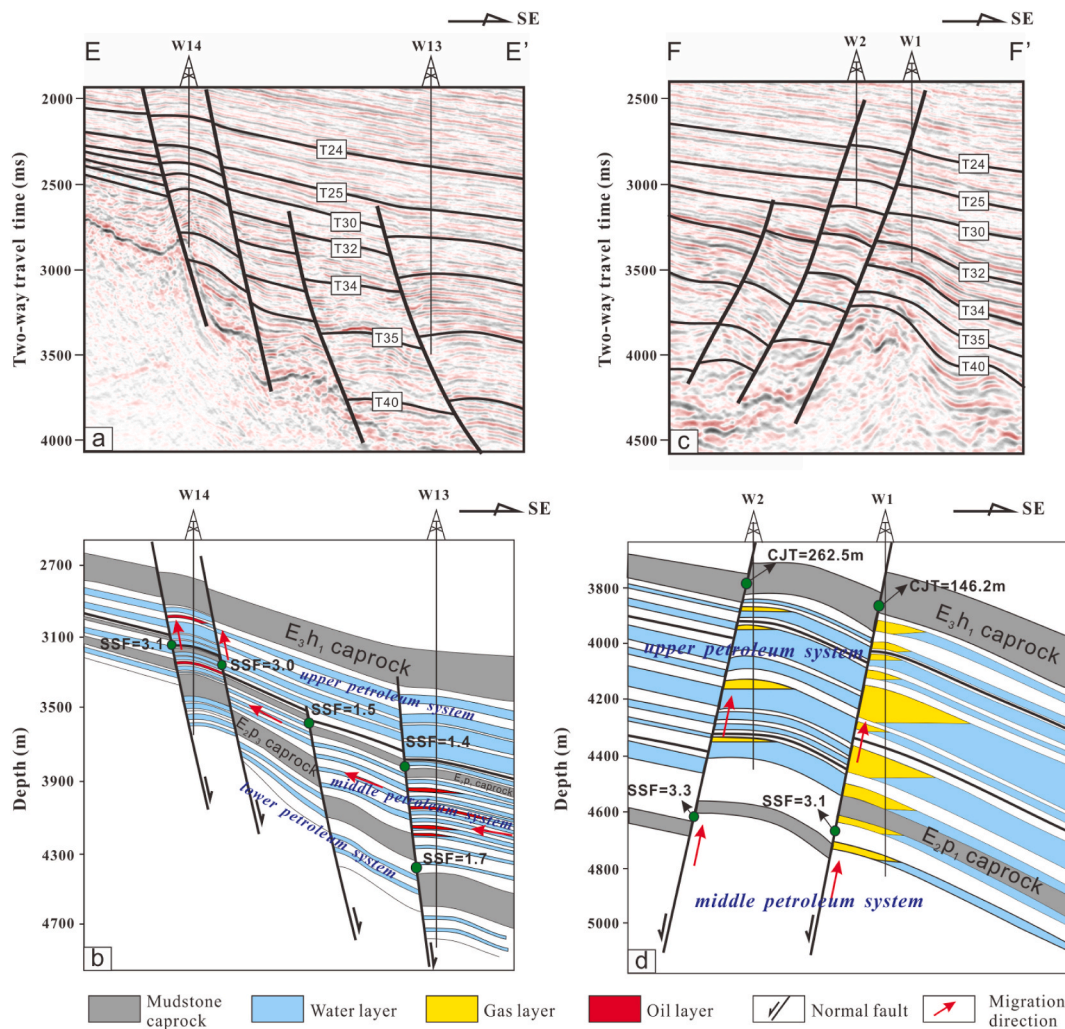
Fig. 12. (a) and (b) show the normal faults, mudstone caprocks, and corresponding hydrocarbon distribution characteristics in the EE′ profile. (c) and (d) show the normal faults, mudstone caprocks, and corresponding hydrocarbon distribution characteristics in the FF′ profile. See Fig. 7a for locations.

caprock was still dominated by brittle-ductile deformation at the TTFA, the thinner thickness (30–100 m) made it more likely to lose its continuity under a large fault displacement. Thus, only the structural center zone of the K gasfield presents a good vertical sealing capacity. For the shallowly buried E_3h_1 caprock with the largest thickness (150–300 m), the brittle deformation before the TTFA made the caprock sealing predominantly determined by mudstone juxtaposition thickness. However, fault activity with a small displacement allowed the cap layer to continuously juxtapose in the lateral direction, so that the E_3h_1 caprock maintained a strong sealing capability. Therefore, based on the determined sealing threshold values of CJT and SSF, hydrocarbon migration and accumulation in the K gasfield occurred via the following process. At the beginning of hydrocarbon charging, the hydrocarbons generated from the WSS migrated laterally to the adjacent structural low zone, the E_2p_1 and E_2p_3 caprocks with a large SSF (>3.0) allowed the hydrocarbons to migrate upwards to the upper petroleum system (such as that in well W1), while the rest of the hydrocarbons continued to migrate laterally to the structurally higher positions. Furthermore, as the mudstone caprock in the structural center zone had a strong sealing capability (SSF<3.0, CJT>56.1 m), vertical leakage of laterally migrated hydrocarbons rarely occurred, and wells W6 and W13 support this interpretation. However, the thinner mudstone caprock in the structural high zone lost its sealing ability due to high SSF values (>3.0), such as those in well W14, which allowed the vertical leakage of hydrocarbons into the upper petroleum system. In this way, the caprock-

sealing characteristics have affected the vertical accumulation and distribution of hydrocarbons in the K gasfield.

4.4. Uncertainty analysis

Quantitative evaluation of caprock-sealing capability is not an exact science. The evaluation models and methods described in the previous section predominantly depend on the precision of fluid pressure prediction, mechanical property estimation, and seismic interpretation models. The definition of the sealing threshold value is simultaneously affected by the amount of statistical data and the detailed judgment of hydrocarbon migration direction. Further uncertainties arise from the brittle-ductile transformation caused by structural uplift during geological history. All these uncertainties should be taken into consideration when quantitatively assessing the sealing capability of caprocks controlled by fault activity.

4.4.1. Fluid pressure prediction

The effective confining pressure of mudstone at different burial depths needs to be calculated in conjunction with fluid pressure. However, the lack of measured pressure data (drill stem test or wireline formation test) commonly prevents a detailed pressure description. In the most ideal case, each continuous prediction model based on geophysical logging can be locally calibrated using the measured pressure data from drilling wells. The prediction model incorporated with

Fig. 13. Summary diagram of the comparison between the current sealing evaluation and caprock sealing evaluation at the TTFA. MT represents the thickness of mudstone, T represents the fault throw, D is the fault displacement, α is the dip angle of fault, CJT$_{threshold}$ is the critical threshold of caprock juxtaposition thickness, and SSF$_{threshold}$ is the critical threshold of the shale smear factor of mudstone caprock.

locally derived parameters ensures the accuracy of the pressure description. Failing this, the pressure prediction model could be calibrated by pressure data from nearby wells or adjacent parts in the same area. However, in frontier exploration areas where pressure data are scarce or do not exist, the fluid pressure of shallow buried mudstone could be equivalent to hydrostatic pressure, but the forecast deviation will appear in the abnormal pressure interval due to the absence of pressure data calibration.

4.4.2. Mechanical property estimation

In practice, core samples of mudstone caprock are mostly unavailable for mechanical laboratory testing, especially in offshore petroliferous basins. As a practical approach to this problem, many empirical equations have been proposed that relate the mechanical properties (internal friction angle, dynamic modulus of elasticity, and cohesion) to the measurable parameters of geophysical logging (such as velocity, density, and porosity). Basically, the mechanical-physical property relationship of a specific mudstone formation should be established based on the calibration of core laboratory tests in the given field.

However, in most cases where there are no laboratory testing data available for calibration, the best way is to use empirical equations for mechanical properties derived from measurable physical properties. Nevertheless, there are many empirical models for different rock types under various geological settings to choose from. Thus, the prediction results may be more likely to deviate from reality when using empirical relationships that do not match the geological conditions of the study area. For this reason, understanding the applicable range of the empirical models and applying them to the most suitable object is the key to diminishing the potential uncertainty in the mechanical parameter estimation of the caprock.

4.4.3. Seismic interpretation model

For the problems associated with quantitatively characterizing caprock sealing, major uncertainty arises from the related basic data obtained through geological interpretation. The major factors affecting the quantitative analysis of caprock sealing are the precision of fault interpretation, displacement measurement and mudstone caprock thickness acquisition. Different qualities of 3D seismic volume will
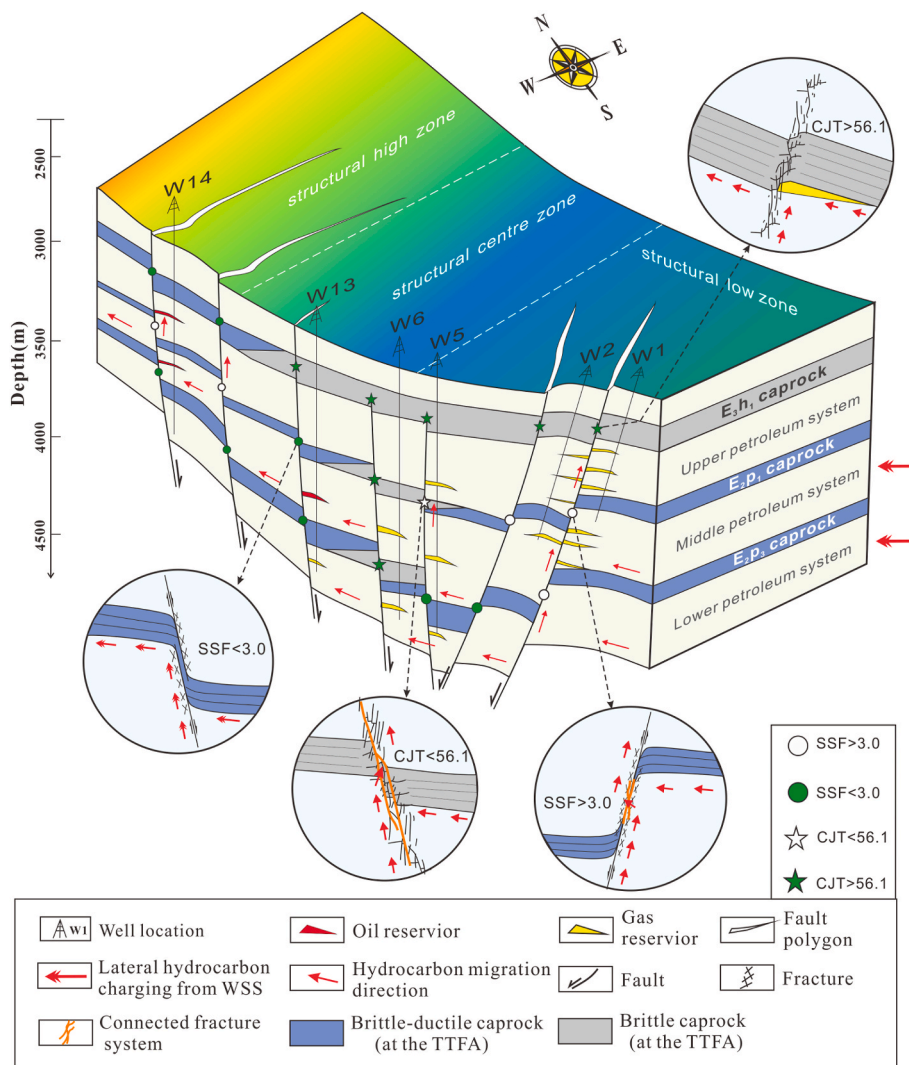
Fig. 14. The conceptual model showing the sealing capability of mudstone caprocks controlled by fault activity and the corresponding hydrocarbon migration and accumulation responses.

contribute to interpretation results, and high-resolution seismic volume subjected to seismic denoising tends to yield more accurate interpretation models. In addition, the fault throw corresponding to different mudstone caprocks should be measured from detailed three-dimensional horizon mapping and fault surfaces. However, due to the difference in vertical resolution between seismic data and logging data, the determination of the mudstone caprock thickness entirely based on seismic data will inevitably deviate from the logging and drilling lithological interpretation to a certain extent.

4.4.4. Sealing threshold value

In this contribution, we used statistical analysis to establish the threshold value between sealing and nonsealing mudstone caprocks. However, two major uncertainties still exist for the scientific definition of the threshold value. One of the factors is the amount of valid data (SSF and CJT) adopted to determine the threshold value of sealing, especially effective data close to the actual threshold. Generally, limited data are more likely to produce a large value interval between sealing and non-sealing, thereby increasing the uncertainty of the threshold value. As the number of available data increases, the uncertainty interval between the sealing and nonsealing of caprock will gradually be diminished, making the threshold value defined based on statistical analysis closer to the actual threshold value. Another factor is the accuracy of judging the hydrocarbon migration direction. The sealing and nonsealing of caprock

depends on whether vertical hydrocarbon leakage occurs. Therefore, the actual evaluation process usually focuses on explaining the current hydrocarbon distribution above and below the caprock from the perspective of vertical migration while ignoring the influence of lateral migration. However, a detailed description of hydrocarbon migration requires systematic geological analyses, such as structural evolutionary history, hydrocarbon generation history, migration carrier analysis, and geochemical tracking. Analyses from different perspectives may lead to different conclusions; therefore, multiple solutions from geological analyses greatly enhance the uncertainty of migration direction judgment.

4.4.5. Structural uplift

In addition to the problems associated with evaluation methods and models, the other major uncertainty comes from the brittle-ductile transformation caused by structural uplift. In this research, we have only discussed normal consolidated rock that has been continuously buried but never uplifted. However, tectonic uplift events are common in basins with complex tectonic evolution. Sedimentary basins that have undergone structural uplift will result in a decrease in confining pressure, which may cause the caprock to transform from a ductile stage to a brittle stage. According to the research of Ingram and Urai (1999) and Nygard et al. (2004, 2006), the uplifted caprock from the maximum burial depth to a shallower structural location belongs to over-consolidated (OC) rocks, and the brittleness of over-consolidated

(OC) rock can be quantitatively characterized by the over-consolidation ratio (OCR). Generally, a higher OCR implies that more fractures could occur during uplift, thereby diminishing the sealing capability of the caprock. Therefore, to accurately determine the effectiveness of the caprock, the uncertain possibility of structural uplift should also be considered when quantitatively assessing caprock sealing.

5. Conclusions

This article proposes a quantitative model for brittle-ductile transition behavior and a reconstruction model of the burial depth to characterize the brittle-ductile stage of caprocks at the termination time of fault activity (TTFA) to evaluate the caprock sealing controlled by fault activity from a dynamic perspective. In the K gasfield in the Xihu Depression, the effective confining pressure of 19 MPa (or 2071.0 m in burial depth) was the critical transition from the brittle to brittle-ductile stage, and the brittle-ductile property reconstruction at the TTFA and matching sealing evaluation have better characterized the effectiveness of the mudstone caprocks. Moreover, the corresponding oil and gas response has revealed that a CJT value of 56.1 m and an SSF value of 3.0 are the thresholds for caprock sealing and nonsealing, which controlled the vertical distribution of hydrocarbons in different structural positions in the K gasfield.

The mathematical models and methods proposed in this research can be effectively improved by enhancing the precision of fluid pressure prediction, mechanical property estimation, and seismic interpretation models. Additionally, in the practice of oil and gas exploration, the quantitative methods and corresponding results derived from this study have great potential for application in the following analyses: (1) combining the dynamic evolution of capillary pressure to analyze the hydrocarbon accumulation scale sealed by the effective caprock; (2) integrating brittle-ductile behavior quantification and over-consolidation ratios (OCR) to understand the caprock-sealing disparity caused by structural uplift; and (3) simulation or prediction of the hydrocarbon accumulation process based on hydrocarbon generation and expulsion history, migration carrier characterization, and caprock-sealing evaluation.

Credit author statement

Fuwei Wang: Methodology, Writing – original draft, Data curation, Conceptualization. **Dongxia Chen:** Conceptualization, Writing – review & editing, Supervision. **Qiaochu Wang:** Conceptualization, Visualization. **Wenlei Du:** Investigation, Software. **Siyuan Chang:** Investigation, Formal analysis. **Cheng Wang:** Investigation, Software. **Ziye Tian:** Investigation, Software. **Ming Cheng:** Investigation. **Dongsheng Yao:** Investigation.

Declaration of competing interest

The authors declare that they have no known competing financial interests or personal relationships that could have appeared to influence the work reported in this paper.

Acknowledgments

References

Abbas, A., Zhu, H.T., Zeng, Z.W., Zhou, X.H., 2018. Sedimentary facies analysis using sequence stratigraphy and seismic sedimentology in the Paleogene Pinghu Formation, xihu depression, east China sea shelf basin. Mar. Petrol. Geol. 93, 287–297.

Alqahtani, A.A., Mokhtari, M., Tutuncu, A.N., Sonnenberg, S., 2013. Effect of mineralogy and petrophysical characteristics on acoustic and mechanical properties of organic rich shale. Unconv Resour Technol Conf 199–411.

Anderson, R.S., 1994. Evolution of the Santa Cruz mountains, California, through tectonic growth and geomorphic decay. J. Geophys. Res.: Solid Earth 99 (B10), 20161–20179.

Bishop, A.W., 1959. The principle of effective stress. Tek. Ukebl. 106 (39), 113–143.

Blair, T.C., Bilodeau, W.L., 1988. Development of tectonic cyclothems in rift, pull-apart, and foreland basins: sedimentary response to episodic tectonism. Geology 16 (6), 517–520.

Bolton, A., Maltman, A., 1998. Fluid-Flow pathways in actively deforming sediments: the role of pore fluid pressures and volume change. Mar. Petrol. Geol. 15 (3), 281–297.

Byerlee, D.J., 1968. Brittle-ductile transition in rocks. J. Geophys. Res. 73, 4741–4750.

Byerlee, J.D., 1978. Friction of rocks. Pure Appl. Geophys. 116, 615–626.

Cai, H., Zhang, J.P., 2013. Characteristics of faults on the Pinghu slope of Xihu sag, the east China Sea Shelf Basin and their sealing capability. Mar Geol Front 29 (4), 20–26 (in Chinese).

Caillet, G., Judge, N.C., Bramwell, N.P., et al., 1997. Overpressure and hydrocarbon trapping in the chalk of the Norwegian central graben. Petrol. Geosci. 3 (1), 33–42.

Cartwright, J.A., Trudgill, B.D., Mansfield, C.S., 1995. Fault growth by segment linkage: an explanation for scatter in maximum displacement and trace length data from the Canyonlands Grabens of SE Utah. J. Struct. Geol. 17 (9), 1319–1326.

Chang, C., Zoback, M.D., Khaksar, A., 2006. Empirical relations between rock strength and physical properties in sedimentary rocks. J. Petrol. Sci. Eng. 51 (3–4), 223–237.

Childs, C., Walsh, J.J., Manzocchi, T., et al., 2007. Definition of a fault permeability predictor from outcrop studies of a faulted turbidite sequence, Taranaki, New Zealand. Geological Society, London, Special Publications 292 (1), 235–258.

Cuisiat, F., Skurtveit, E., 2010. An experimental investigation of the development and permeability of clay smears along faults in uncemented sediments. J. Struct. Geol. 32 (11), 1850–1863.

Davatzes, N.C., Aydin, A., 2005. Distribution and nature of fault architecture in a layered sandstone and shale sequence: an example from the Moab fault, Utah. Fluid flow and petroleum traps. AAPG Memoir 85, 153–180.

Deere, D.U., Miller, R.P., 1966. Engineering Classification and Index Properties for Intact Rock. Teck. Report. AFWL-TR Kirtland Base, New Mexico.

Dott, R.H., Reynolds, M.J., 1969. Source book for petroleum geology. In: Tulsa, AAPG Memoir, vol. 5, p. 471.

Doughty, P.T., 2003. Clay smear seals and fault sealing potential of an exhumed growth fault, Rio Grande rift, New Mexico. AAPG (Am. Assoc. Pet. Geol.) Bull. 87 (3), 427–444.

Duan, M., Ye, J., Wu, J., Shan, C., Lei, C., 2017. Overpressure formation mechanism in xihu depression of the east China sea shelf basin. Earth Sci. 42 (1), 119–129 (in Chinese).

Engelder, T., Lacazette, A., 1990. Natural Hydraulic Fracturing. Rock joints, Rotterdam, AA Balkema, pp. 35–44.

Faerseth, R.B., 2006. Shale smear along large faults: continuity of smear and the fault seal capacity. J. Geol. Soc. 163 (5), 741–751.

Fossen, 2010. Structural Geology. Cambridge University Press, pp. 119–185.

Fu, X.F., Jia, R., Wang, H.X., Wu, T., Meng, L.D., Sun, Y.H., 2015. Quantitative evaluation of fault-caprock sealing capacity: a case from dabei-kelasu structural belt in Kuqa Depression, Tarim Basin, NW China. Petrol. Explor. Dev. 42 (3), 329–338.

Fu, X.F., Yan, L.Y., Meng, L.D., Liu, X.B., 2019. Deformation mechanism and vertical sealing capacity of fault in the mudstone caprock. J. Earth Sci. 30 (2), 367–375.

Fuchs, R., Hamilton, W., 2006. New depositional architecture for an old giant: the Matzen Field, Austria. In: Golonka, J., Picha, F.J. (Eds.), The Carpathians and Their Foreland: Geology and Hydrocarbon Resources, vol. 84. AAPG Memoir, pp. 205–219 (Chapter 6).

Fuenkajorn, K., Sriapai, T., Samsri, P., 2012. Effects of loading rate on strength and deformability of maha sarakham salt. Eng. Geol. 135–136 (none), 10–23.

Fulljames, J.R., Zijerveld, L.J.J., Franssen, R.C.M.W., 1997. Fault seal processes: systematic analysis of fault seals over geological and production time scales. In: Møller-Pedersen, P., Koestler, A.G. (Eds.), 7. Norwegian Petroleum Society Special Publications, pp. 51–59.

Gartrell, A., Bailey, W.R., Brincat, M., 2006. A new model for assessing trap integrity and oil preservation risks associated with postrift fault reactivation in the Timor Sea. AAPG (Am. Assoc. Pet. Geol.) Bull. 90 (12), 1921–1944.

Goetze, C., 1971. High temperature rheology of Westerly granite. J. Geophys. Res. 76 (5), 1223–1230.

Grunau, H.R., 1987. A worldwide look at the cap-rock problem. J. Petrol. Geol. 10 (3), 245–265.

Gutierrez, M., Øino, L.E., Nygard, R., 2000. Stress-dependent permeability of a demineralised fracture in shale. Mar. Petrol. Geol. 17 (8), 895–907.

Hamami, M., 1999. Simultaneous effect of loading rate and confining pressure on the deviator evolution in rock salt. Int. J. Rock Mech. Min. Sci. 36 (6), 827–831.

Hao, F., Zhu, W.L., Zou, H.Y., Li, P.P., 2015. Factors controlling petroleum accumulation and leakage in overpressured reservoirs. AAPG (Am. Assoc. Pet. Geol.) Bull. 99 (5), 831–858.

He, G.Y., Zhang, W.H., 1997. Review on study and tendency of cap rocks. Glob. Geol. 16, 28–33 (in Chinese).

Horsrud, P., 2001. Estimating mechanical properties of shale from empirical correlations. SPE Drill. Complet. 16 (1), 68–73.

Hottman, C.E., Johnson, R.K., 1965. Estimation of formation pressures from log-derived shale properties. J. Petrol. Technol. 17 (6), 717–722.

Ingram, G.M., Urai, J., Naylor, M.A., 1997. Sealing processes and top seal assessment. Norwegian Petroleum Society Special Publications 7 (97), 165–174.

Ingram, G.M., Urai, J.L., 1999. Top-seal leakage through faults and fractures: the role of mudrock properties. Geological Society, London, Special Publications 158 (1), 125–135.

Jackson, C.A.L., Rotevatn, A., 2013. 3D seismic analysis of the structure and evolution of a salt-influenced normal fault zone: a test of competing fault growth models. J. Struct. Geol. 54, 215–234.

Jin, Z.J., Yuan, Y.S., Liu, Q.Y., Wo, Y.J., 2013. Controls of Late Jurassic-Early Cretaceous tectonic event on source rocks and seals in marine sequences, South China. Sci. China 56 (2), 228–239.

Jin, Z.J., Yuan, Y.S., Sun, D.S., Liu, Q.Y., Li, S.J., 2014. Models for dynamic evaluation of mudstone/shale cap rocks and their applications in the lower paleozoic sequences, Sichuan Basin, SW China. Mar. Petrol. Geol. 49, 121–128.

Kohlstedt, D.L., Evans, B., Mackwell, S.J., 1995. Strength of the lithosphere: constraints imposed by laboratory experiments. J. Geophys. Res.: Solid Earth 100 (B9), 17587–17602, 1995.

Lal, M., 1999. Shale stability: drilling fluid interaction and shale strength. In: SPE Latin American and Caribbean Petroleum Engineering Conference Held in Caracas, Venezuela.

Lehner, F.K., Pilaar, W.F., 1997. The emplacement of clay smears in synsedimentary normal faults: inferences from field observations near frechen, Germany. Norwegian Petroleum Society Special Publication 7, 15–38.

Li, C.L., Kong, X.Y., Xu, X.Z., Li, P.C., 1999. Double effective stress of porous media. Nat. Mag. 21 (5), 288–292.

Lindsay, N.G., Murphy, F.C., Walsh, J.J., Watterson, J., 1993. Outcrop studies of shale smear on fault surfaces. Int. Assoc. Sedimentol. Spec. Publ. 15, 113–123.

Lü, Y.F., Fu, G., Gao, D.L., 1996. Study on the Cap Rock of Reservoir. Petroleum Industry Press, Beijing, pp. 118–120.

Lü, Y.F., Sha, Z.X., Fu, X.F., Fu, G., 2007. Quantitative evaluation method for fault vertical sealing ability and its application. Acta Pet. Sin. 28 (5), 34–38 (in Chinese).

Magara, L.J., 1968. Compaction and migration of fluids in Miocene mudstone, Nagaoka plain, Japan. AAPG (Am. Assoc. Pet. Geol.) Bull. 52 (12), 2466–2501.

Manzocchi, T., Childs, C., Walsh, J.J., 2010. Faults and fault properties in hydrocarbon flow models. Geofluids 10 (1–2), 94–113.

McNally, G.H., 1987. Estimation of coal measures rock strength using sonic and neutron logs. Geoexploration 24, 381–395.

Mou, Z.H., 1993. A new method to calculate the ancient thickness of sedimentary sequences. Exp. Pet. Geol. 15 (4), 414–422 (in Chinese).

Nygard, R., Gutierrez, M., Bratli, R.K., Høeg, K., 2006. Brittle-ductile transition, shear failure and leakage in shales and mudrocks. Mar. Petrol. Geol. 23, 201–212.

Nygard, R., Gutierrez, M., Gautam, R., Høeg, K., 2004. Compaction behavior of argillaceous sediments as function of diagenesis. Mar. Petrol. Geol. 21, 349–362.

Perrier, R., Quiblier, J., 1974. Thickness changes in sedimentary layers during compaction history: methods for quantitative evaluation. AAPG (Am. Assoc. Pet. Geol.) Bull. 58 (3), 507–520.

Petley, D.N., 1999. Failure envelopes of mudrocks at high confining pressures. Geological Society, London, Special Publications 158 (1), 61–71.

Pierce, W.H., 1993. Southern Arabian Basin oil habitat: seals and gathering areas. In: Paper Presented at the Middle East Oil Show, Bahrain.

Runar, N., Marte, G., Rolf, K.B., Kaare, H., 2006. Brittle-ductile transition, shear failure and leakage in shales and mudrocks. Mar. Petrol. Geol. 23, 201–212.

Rykkelid, E., Fossen, H., 2002. Layer Rotation around vertical fault overlap zones: observations from seismic data, field examples, and physical experiments. Mar. Petrol. Geol. 19 (2), 181–192.

Schowalter, T.T., 1979. Mechanics of secondary hydrocarbon migration and entrapment. AAPG (Am. Assoc. Pet. Geol.) Bull. 63 (5), 723–760.

Schowalter, T.T., 1981. Prediction of caprock seal capacity: abstract. AAPG (Am. Assoc. Pet. Geol.) Bull. 65, 987–988.

Shan, C., Ye, J.R., Cao, Q., Lei, C., Peng, Y., Tian, Y., 2015. Controlling factors for gas accumulation in kongqueting gas field of Xihu Sag. Mar. Geol. Quat. Geol. 35 (1), 135–144 (in Chinese).

Shao, X.J., Liu, Z., Cui, W.F., 1999. Restoration of the paleo-burial depth of strata in deposition basin. Petrol. Explor. Dev. 26 (3), 33–35 (in Chinese).

Sibson, R.H., 1996. Structural permeability of fluid-driven fault-fracture meshes. J. Struct. Geol. 18 (8), 1031–1042.

Song, X.Y., Chu, C.L., Rui, Z.F., 2010. Structural framework and evolution of xihu sag in east China Sea Basin. Geol. J. China Univ. 16 (1), 86–93 (in Chinese).

Sperrevik, S., Færseth, R.B., Gabrielsen, R.H., 2000. Experiments on clay smear formation along faults. Petrol. Geosci. 6 (2), 113–123.

Su, A., Chen, H.H., Ma, Y.H., Zhan, H.Y., Yang, W.S., 2015. Geologic conditions and main controlling factors of gas washing in Kongqueting region in Xihu Depression, Eastern Sea Basin. Nat. Gas Geosci. 26 (2), 292–300 (in Chinese).

Su, A., Chen, H.H., Zhao, J.X., Zhang, T.W., Feng, Y.X., Wang, C.W., 2020. Natural gas washing induces condensate formation from coal measures in the Pinghu Slope Belt of the Xihu Depression, East China Sea Basin: insights from fluid inclusion, geochemistry, and rock gold-tube pyrolysis. Mar. Petrol. Geol. 118.

Sun, D.Z., Zhang, H.S., Duan, F.F., Yan, W.F., Shi, X.C., 2016. Experimental study on mechanics and drillability of lower strata rock in central subsag of Xihu sag. China Offshore Oil Gas 28 (1), 93–97 (in Chinese).

Terzaghi, K., 1923. Die Berechnung der Durchassigkeitsziffer des Tones aus dem Verlauf der hydrodynamischen Spannungserscheinungen. Akademie der Wissenschaften in Wien 132 (3/4), 125–138.

Vrolijk, P.J., Urai, J.L., Kettermann, M., 2016. Clay smear: review of mechanisms and applications. J. Struct. Geol. 86, 95–152.

Wang, F.W., Chen, D.X., Wang, Q.C., Shi, X.B., Xie, G.J., Wang, Z.Y., Li, J.H., Liao, W.H., 2020. Evolution characteristics of transtensional faults and their impacts on hydrocarbon migration and accumulation: a case study from the Huimin Depression, Bohai Bay Basin. Mar. Petrol. Geol. 120.

Wang, F.W., Chen, D.X., Du, W.L., Zeng, J.H., Wang, Q.C., Tian, Z.Y., Chang, S.Y., Jiang, M.Y., 2021. Improved method for quantitative evaluation of fault vertical sealing: a case study from the eastern Pinghu slope belt of the xihu depression, east China sea shelf basin. Mar. Petrol. Geol. 132.

Wang, H.X., Wu, T., Fu, X.F., Liu, Bo, Wang, S., Jia, R., Zhang, C., 2019. Quantitative determination of the brittle-ductile transition characteristics of caprocks and its geological significance in the kuqa depression, tarim basin, western China. J. Petrol. Sci. Eng. 173, 492–500.

Wang, L.J., Liu, X.J., Han, L., Zhou, G.Y., Xie, L.X., 2007. The experimental study of elastic modulus and Poisson ratio based on the sonic time difference. J. Southwest Petrol. Univ. 29 (S1), 19–21 (in Chinese).

Watts, N., 1987. Theoretical aspects of cap-rock and fault seals for single- and two-phase hydrocarbon columns. Mar. Petrol. Geol. 4 (4), 274–307.

Webster, M., O'Connor, S., Pindar, B., Swarbrick, R., 2011. Overpressures in the Taranaki basin: distribution, causes, and implications for exploration. AAPG (Am. Assoc. Pet. Geol.) Bull. 95 (3), 339–370.

Wu, J.W., Zhang, Q., Wu, S.G., Lü, F.L., Wang, B., He, X.S., Mao, C.L., 2013. Reservoir characteristics and controls of huge oil fields in the South China Sea. Prog. Geophys. 28 (6), 3106–3116 (in Chinese).

Xu, H.Y., George, S.C., Hou, D.J., Cao, B., Chen, X.D., 2020. Petroleum sources in the Xihu Depression, East China Sea: evidence from stable carbon isotopic compositions of individual n-alkanes and isoprenoids. J. Petrol. Sci. Eng. 190.

Xue, Y.A., Wang, D.Y., 2020. Formation conditions and exploration direction of large natural gas reservoirs in the oil-prone bohai bay basin, east China. Petrol. Explor. Dev. 47 (2), 58–69.

Yang, C.H., Zeng, G.D., Li, S.Q., Liang, R.B., 2014. Fault development characteristics and hydrocarbon accumulation in pingbei area of xihu sag, east China sea. Petrol. Geol. Exper. 36 (1), 68–69+82 (in Chinese).

Ye, J., Qing, H., Bend, S.L., Gu, H., 2007. Petroleum systems in the offshore xihu basin on the continental shelf of the east China sea. AAPG (Am. Assoc. Pet. Geol.) Bull. 91 (8), 1167–1188.

Yielding, G., 2002. Shale Gouge ratio-calibration by geohistory. Norwegian Petroleum Society Special Publications 11, 1–15.

Yielding, G., Freeman, B., Needham, D.T., 1997. Quantitative fault seal prediction. AAPG (Am. Assoc. Pet. Geol.) Bull. 81 (6), 897–917.

Yuan, B.C., Qian, Y.Z., 1986. Method of "recovery layer by layer" for calculation the paleothickness of sedimentary layer. Exp. Pet. Geol. 8 (3), 64–73 (in Chinese).

Zhang, J., Lu, Y., Krijgsman, W., Liu, J.H., Li, X.Q., Du, X.B., Wang, C., Liu, X.C., Feng, L., Wei, W., Lin, H., 2018. Source to sink transport in the oligocene Huagang Formation of the xihu depression, east China sea shelf basin. Mar. Petrol. Geol. 98, 733–745.

Zhang, Y.X., Ye, J.R., Su, K.L., Li, L.X., Xu, J.J., 2009. The burial history and evolution of Xihu Depression. Geotect. Metallogenia 33 (2), 215–223 (in Chinese).

Zhao, J., 2000. Applicability of Mohr-Coulomb and Hoek-Brown strength criteria to the dynamic strength of brittle rock. Int. J. Rock Mech. Min. Sci. 37 (7), 1115–1121.